ABSTRACT

Title of the Thesis: LIFE CONSUMPTION MONITORING FOR ELECTRONICS

Degree Candidate: Satchidananda Mishra, Master of Science, 2003

Thesis directed by: Professor Michael Pecht
Department of Mechanical Engineering

Life consumption monitoring is a method to assess product's reliability based on its remaining life in a given life cycle environment. The life consumption monitoring process involves continuous or periodic measurement, sensing, recording, and interpretation of physical parameters associated with a system's life cycle environment to quantify the amount of degradation.

This thesis explains a life consumption monitoring methodology for electronic products, which includes failure modes, mechanisms and effects analysis (FMMEA), virtual reliability assessment, monitoring product parameters, data simplification, stress and damage accumulation analysis and remaining life estimation. It presents two case studies to estimate the remaining life of identical circuit card assemblies in an automobile underhood environment using the life consumption monitoring methodology. Failure modes, mechanisms, and effects analysis along with virtual reliability assessment is used to determine the dominant failure mechanism in the given life cycle environment. Temperature and vibration are found to be the environmental factors, which could potentially cause malfunction of the circuit card assembly through solder joint fatigue.

Temperature sensor and accelerometers are used along with a data logger to monitor and record the environmental loads during the experiment. A data simplification scheme is used to make the raw sensor data suitable for further processing. Stress and damage models are used to estimate the remaining life of the circuit card assembly based on the simplified data. Performances of the test board assemblies are monitored through resistance monitoring. The life cycle environment and results for the case studies are compared with each other. The estimated results are also compared with experimental life results.

LIFE CONSUMPTION MONITORING FOR ELECTRONICS

By

Satchidananda Mishra

Thesis submitted to the Faculty of the Graduate School of the
University of Maryland, College Park in partial fulfillment
of the requirements for the degree of
Master of Science
2003

Advisory Committee:

Professor Michael Pecht, Chair
Associate Professor Patrick McCluskey
Associate Professor Peter Sandborn

PREFACE

In today's world, increasing global competition along with consumers' perceptions toward performance, quality, reliability, safety, and environmental considerations are compelling manufacturers to improve their design for higher reliability in field applications. In electronics industry, product development trends have supported this requirement through rapid technological changes resulting in rapid market growth. However, as manufacturers try to keep pace with performance requirements of modern electronic industry, reliability is being traded-off at an affordable cost. Intense market competition has reduced time-to-market for electronics products tremendously thereby providing less time for extensive reliability testing. There has been a continuous transition in the electronics industry from military-specification parts to commercial-off-the-shelf (COTS) parts, many of which are now targeted for lifetimes in the 5 to 7 year range. Wearout of electronics parts has become a relevant concern with this transition. Hence there is a need for today's companies to consider novel approaches to improve design and maintain operational efficiency of their products in field applications to ensure customer satisfaction.

Health monitoring has emerged as a promising alternative to traditional reliability prediction, scheduled maintenance, and run-to-failure operations. Health monitoring is the method of monitoring product reliability in terms of its health in the life cycle environment. Life consumption monitoring (LCM) is a health monitoring method to assess product's reliability based on its remaining life in a given life cycle environment. The aim of this thesis is to develop and demonstrate a life consumption monitoring

methodology to determine the remaining life and reliability of an electronic product based on monitored environmental and operational data. Life consumption monitoring is a prognostic process unlike many other health monitoring approaches. A well-designed maintenance procedure based on life consumption monitoring can be used to predict and prevent system failure and hence to reduce operating costs.

Chapter 1 discusses the concept and motivation behind the reliability prediction practices followed in industry. This chapter highlights the drawbacks of current reliability prediction techniques and explains health monitoring as a solution to the reliability prediction challenge. The approaches adopted for health and life consumption monitoring are described along with various examples.

Chapter 2 describes a physics-of-failure-based life consumption monitoring to determine the remaining life of an electronic product. The life consumption monitoring process involves continuous or periodic measurement, sensing, recording, and interpretation of physical parameters associated with a system's life cycle environment to quantify the amount of system degradation. The process is documented in the form of a flowchart, which includes failure modes, mechanisms, and effects analysis (FMMEA), virtual reliability assessment, monitoring product parameters in the product's life cycle environment, data simplification, stress and damage accumulation analysis and remaining life estimation.

Chapter 3 describes two case studies to demonstrate the developed life consumption monitoring methodology. For the case studies, two circuit card assemblies were mounted under-the-hood of an automobile. Failure modes, mechanisms, and effects analysis (FMMEA) was conducted along with a virtual reliability assessment for the

circuit card assembly in the given life cycle environment, which revealed that solder joint fatigue is the dominant failure mechanism. The environmental parameters that can cause damage are identified as temperature, and vibration. A suitable data simplification scheme was developed to make the sensor data suitable for input to solder joint fatigue models. The identified environmental parameters were monitored and recorded with the help of sensors and a battery powered data logger. The collected and simplified data was used with stress and damage models using the calcePWA analysis software to estimate the remaining life. The actual life of the circuit card assemblies were checked through resistance monitoring and compared with the estimated life.

Chapter 4 presents a summary and some discussion on the life consumption monitoring methodology described in the thesis. Chapter 5 highlights the specific contributions made in this thesis.

ACKNOWLEDGEMENTS

I wish to express my sincere gratitude to Dr. Michael Pecht, Dr. Peter Sandborn, and Dr. Patrick McCluskey of the University of Maryland, College Park for their advice and support during the course of this thesis and my stay at the University of Maryland. I am grateful to Dr. Diganta Das, Dr. Miky Lee, Dr. Sanka Ganesan, Keith Rogers, and Dan Danahoe of CALCE center at the University of Maryland, without whose help this thesis would not have reached a fruitful completion. I also wish to express my gratitude to Mr. Doug Goodman from Ridgetop Group Inc., Mr. Bart Feys from Dallas Instruments, and Mr. Paul Macmillan from ACI-AppliCAD Inc.

I express my special thanks to my colleagues Yuki Fukuda, Jeremy Cunningham, Sathyanarayan Ganesan, Niranjan Vijayragavan, Yu-Chul Hwang, Paul Casey, Anoop Rawat, Vidyasagar Shetty, Lewis Gershan, Ji Wu, Sanjay Tiku, Subramaniam Rajagopal, Leila Jannessari, Joseph Varghese, Arindam Goswami, Ricky Valentin, Karumbu, Kaushik Ghosh, who have always been helpful to me during my thesis work.

TABLE OF CONTENTS

LIST OF TABLES

LIST OF FIGURES

1 INTRODUCTION

Reliability is defined as the ability of a product to perform as intended (i.e., without failure and within specified performance limits) for a specified time, in its life cycle application environment. During the past 25 years, there has been a lot of improvement in the reliability of electronic products to keep pace with the increased warranties and the possible liabilities of product failures. Various technology improvements including semiconductor manufacturing processes have continuously helped to increase device reliability. However, there has been continuous shrinking of the feature sizes for electronic devices along with improved performance requirements. In fact, according to Moore's law number of transistors in a given semiconductor has been doubling every eighteen months. This trend has decreased the device dimensions thereby resulting in higher electric fields and higher localized heating. Surface mount technology (SMT) has become a common practice to take into account the higher I/O requirement, which has made interconnects more vulnerable to harsh environments. In other words, as manufacturers try to keep pace with performance requirements, reliability of electronic systems is getting traded-off for increased functionality at an affordable cost.

There has been intense competition among rival companies based on cost and quality of electronics products. Increasing market competition and customers' expectation for latest technology has reduced the allowable "time to market" in electronics industry tremendously. With reduction in allowable time for the product development cycles, there is less opportunity for extensive reliability testing. As a result, outputs from the current reliability assessment schemes, which are based on extensive reliability trials, may not satisfy the customer requirements. Failure to resolve this issue

can result in high risk of in-service availability and inflated life support costs for electronic systems.

The modern electronics industry is more and more being driven by the consumer electronics segment as compared to space, military, avionics and oil-drilling segment (i.e., the low volume complex electronics or LVCES industry). This has compelled the LVCES industry to adapt to the commercial-off-the-shelf (COTS) parts instead of traditional military-specification parts. With this transition from military-specification parts to COTS parts, many of which are now targeted for lifetimes in the 5 to 7 year range, wearout of electronics parts is becoming a concern.

There has been a constant need for the maintenance strategies to be more proactive based on in-service reliability of the products. By knowing whether and, more importantly, when maintenance is needed, production or operation schedules can be synchronized, and the cost of maintenance can be reduced. Hence there is a need for the companies to consider various approaches in order to improve reliability and maintain the operational efficiency of their products in the field applications including in-service reliability monitoring.

In-service reliability of a product is dependent on the environmental and operational conditions of the product in its field applications. Traditionally, reliability of electronic products has been predicted without keeping in mind the actual environmental and operational parameters in its life cycle environment. Current data collection schemes for reliability assessment are often designed before in-service operational and environmental aspects of the system are entirely understood. Further the allowable time

for reliability trials are reducing because of reduction in product development cycles, thereby causing lack of suitable test data.

In summary, today's organizations are faced with the challenge of maintaining electronic product reliability with increased performance requirements, increased market competition, and less allowable time-to-market. There is a continuous demand to lower maintenance costs and to hasten operational readiness/responsiveness.

Health monitoring has emerged as a promising alternative to traditional reliability prediction, scheduled maintenance, and run-to-failure operations. Health monitoring is the method of monitoring product reliability in terms of its health in the life cycle environment. Life consumption monitoring (LCM) is a health monitoring method to assess product's reliability based on its remaining life in a given life cycle environment. The life consumption monitoring process involves continuous or periodic measurement, sensing, recording, and interpretation of physical parameters associated with a product's life cycle environment to quantify the amount of degradation. This thesis describes the concept and various aspects of life consumption monitoring along with two case studies.

1.1 Reliability Prediction of Electronics

Reliability is defined as the ability of a product to perform as intended (i.e., without failure and within specified performance limits) for a specified time, in its life cycle application environment. An efficient reliability prediction can be used for numerous purposes, including the following [1]

- Comparisons of the designs and products
- Methods to identify potential reliability improvement opportunities
- Logistics support

  - Forecast warranty and life cycle costs
  - Spare parts provisioning
  - Availability
- Safety analysis
- Mission reliability estimation
- End item reliability estimation
- Prediction of reliability performance

IEEE standard 1413 [1], titled "Standard Methodology for Reliability Prediction and Assessment for Electronic Systems and Equipment" presents the key parameters of importance for reliability prediction include structural architecture, material properties, fabrication and assembly processes, and the life cycle environment.

Defining and characterizing the product life cycle environment is often the most uncertain input into a reliability prediction scheme. Product life cycle environment typically includes storage, transportation, handling and application scenario of the product. It also describes the expected severity and duration of the load conditions for each scenario [2], [3]. Load conditions for an electronic product include temperature, humidity, vibration or shock loads, contaminants, radiation levels, electromagnetic interference and loads caused by operational parameters such as current, power and heat dissipation. Life cycle environment characterization also requires knowledge of parameters like the application length, the number of applications in the expected life of the product, and the product utilization or non-utilization profile (storage, testing, transportation).

The common practice of design has been to provide a safety margin, i.e., designing for a high product load and recommending operation at a lower value, due to uncertainties regarding the actual life cycle loads for a product [4]. If the actual life cycle loads are different from the designed ones, this design practice can lead to costly over design or hazardous under design, and consequently, increased costs.

1.2 Health Monitoring

Health monitoring is one of the emerging and most promising developments in the evolution of in-service reliability assessment and maintenance practices. A product's health is the extent of degradation or deviation from its "normal" operating state. Hence health monitoring is based on the condition of the actual system or equipment concerned, not on the statistical mean. By determining whether and, more importantly, when failure can occur, procedures can be developed to mitigate, manage or maintain the product [5]. An efficient health monitoring scheme can be used to [6]:

- Reduce lost output penalties
- Reduce forced outage repair and labor costs
- Reduce spares holdings
- Reduce severity of failures
- Improve safety margins
- Reduce insurance premiums
- Extend maintenance cycles
- Maintain the effectiveness of equipment through timely repair actions
- Improve repair quality
- Increase profitability

Methods employed for health monitoring can include non-destructive tests (e.g., ultrasonic inspection, liquid penetrant inspection, and visual inspection) and operating parameter monitoring (e.g., vibration monitoring, oil consumption monitoring and thermography (infrared) monitoring) [7]. Predictive or prognostic health monitoring methods involve monitoring of the life cycle environment of the product (e.g., temperature, humidity, shock, vibration, current, power, heat dissipation) to predict when the product is going to fail in real life.

Health monitoring has been used for both electrical and mechanical systems for reliability prediction and hence reduction in maintenance expenses. An example of the monetary benefit of health monitoring was presented in the context of corrosion in a workshop on condition-based maintenance (CBM) on November 17-18, 1998 in Atlanta, organized by the Advanced Technology Program (ATP) of the National Institute of Standards and Technology (NIST) [8]. It was stated that if corrosion could be measured directly at a refinery plant, the downtime for maintenance could be reduced from every year to potentially every 3 years. Since a typical maintenance period is two weeks to a month (about 10% of the available operating time), an economic value can be assigned to a reduction in downtime. However, offsetting maintenance costs is probably not the primary economic driver for CBM. Instead, it should be looked at as an integral part of a business strategy for profitability. In the case of CBM, it contributes to maximum up time (capacity) with reduced operating costs.

There are some technical barriers for implementation of health monitoring, which include the inability to continually monitor a system and accurately predict the remaining useful life. Further the use of health monitoring in real life can be more appreciated if it

can help in learning and identifying impending failures for a system as well as recommending an action.

1.3 Approaches for Health Monitoring

Health monitoring is the method of evaluating reliability in terms of product's health in its life cycle environment. Health monitoring methods can be broadly classified into two categories, i.e., current condition monitoring and life consumption monitoring.

1.3.1 Current Condition Monitoring

Current condition monitoring is a method of evaluating the product's operating state in terms its physical degradation (e.g., cracks, corrosion, delamination), electrical degradation (e.g., increase in resistance, increase in threshold voltage), and performance degradation (e.g., shift of the product's operating parameters from expected values). The objective of condition monitoring (also called condition-based maintenance) is to accurately detect the current state of electrical and mechanical systems and enable the user to make a decision on whether to perform maintenance. Hence condition monitoring is mainly a diagnostic activity. This helps to prevent operational deficiencies and failures, eliminates costly periodic maintenance, and reduces the likelihood of machinery failures.

1.3.2 Life Consumption Monitoring

Life consumption monitoring (LCM) is a method to assess product's reliability based on its remaining life in a given life cycle environment. In life consumption monitoring, product's reliability can be assessed by comparing the remaining life of the product with estimated total life. The life consumption monitoring process involves continuous or periodic measurement, sensing, recording, and interpretation of physical

parameters associated with a system's life cycle environment to quantify the amount of system degradation.

1.4 Current State of Health Monitoring Research

Most of the work on health monitoring available in literature focuses on diagnostic or condition monitoring of various mechanical (metals and composites) structures. This is often sited as "structural health monitoring". Typical methods used for condition monitoring include

- Visual inspection
- Optical fibers [9], [10], [11]
- Eddy current [12]
- Acoustic emission [13]
- Vibration signatures and modal analysis [14], [15], [16]
- Piezoelectric materials [17], [18]

Several organizations, professional societies and universities are involved in activities related to health monitoring. The following section gives a listing of some of the leading groups involved in health monitoring research:

- Condition Monitoring and Diagnostic Engineering Management (COMADEM) [19]
    - Consultancy program on different aspects of condition and diagnostic monitoring focusing on proactive integrated maintenance management.
    - Publishers of "International Journal of COMADEM" dedicated to sensor technology, structural health monitoring and machinery/process health monitoring
- Society for Machinery Failure Prevention Technology (MFPT) is a professional society focused on sensors technology, condition monitoring, predictive maintenance,

prognostics technology, condition based maintenance, nondestructive evaluation and testing, life extension and integrated diagnostics in conjunction with the annual meeting [20].

- The National Aeronautics and Space Administration (NASA)
  - Health monitoring for aviation safety program (AvSP) which includes monitoring fuel flow, rotor speeds, oil temperature/ pressure, engine vibration [21]
  - Efficient checkout, testing and monitoring of space transportation vehicles, subsystems and components before, during and after operation under the vehicle health monitoring (VHM) program [22].
  - Develops smart sensors for health monitoring, e.g., solenoid health monitor for valve health monitoring and failure prediction.
- Office of Naval Research conducts research for on-board mechanical diagnostics and vehicle health monitoring (integrated avionics) for improved operational effectiveness of air vehicles with increased capability, range, speed, time-on-station, and carrier suitability [23].
- Department of Defense (DoD) has a prognostics health management (PHM) program for joint strike fighter (JSF) [24]
- QinetiQ, UK
  - Vehicle health and usage monitoring system (vHUMS) program that uses various sensor technologies, data analysis and reporting tools [25]
  - Integrated engine management program using condition monitoring [26]
- UK Ministry of Defense (MoD) - Engine health monitoring systems [27]

- US Army Material Systems Analysis Activity (AMSAA) – Physics-of-failure approach for reliability modeling [28]
- CALCE EPSC at University of Maryland conducts research on diagnostic and prognostic health monitoring focusing on electronics [29]
- Pennsylvania State University Applied Research Laboratory (ARL) [30]

1.5 Health Monitoring Examples

An example of condition monitoring in mechanical systems is applied in the ETOPS (Extended-range Twin-engine Operations) program. ETOPS restriction, formalized under US FAA Regulations in 1953, prohibits passenger carrying aircraft with only two engines from flying any route more that a given single-engine flying time from a suitable and open landing site. Gradual relaxation in this rule has resulted from improvements in health monitoring technologies, which now provide the continuous monitoring of critical aircraft systems necessary to identify problems before they affect aircraft operation or safety along with reductions in engine in-flight shutdown rates. The ETOPS philosophy is a real-time approach to maintenance and includes continual monitoring of application conditions to identify problems. Two typical examples of ETOPS are engine condition monitoring (ECM) and oil consumption monitoring. ETOPS operators are required to use ECM programs to monitor adverse trends in engine performance and execute maintenance to avoid serious failures (e.g., those that could cause in-flight shutdowns, diversions, or turnbacks). The ECM programs allow for monitoring of engine parameters such as exhaust temperature, fuel and oil pressures, and vibration. In some cases, oil consumption data and ECM data can be correlated to define

certain problems. Any engine deterioration that might affect ETOPS operations is monitored through a disciplined data collection and analysis program [31].

Built-in-test (BIT) is a condition monitoring technique used for electronics that uses hardware-software diagnostic mean to identify and locate faults. Two types of BIT concepts are employed in electronic systems, interruptive BIT (I-BIT) and continuous BIT (C-BIT). The concept of I-BIT is that normal equipment operation is suspended during BIT operation. Such BITs are typically initiated by the operator or during a power-up process. The concept of C-BIT is that equipment is monitored continuously and automatically without affecting normal operation [32].

JDIS (Joint Distributed Information System), another example of health monitoring scheme applied to mechanical systems. JDIS can anticipate maintenance and repair needs to ensure that equipment and personnel are available precisely when needed [33]. It can reduce the time taken to deliver aircraft replacement parts to be hours, as compared to weeks or months under current practices. During a demonstration, Boeing simulated how a network of computers and aircraft sensors can trigger an autonomic response to a pending maintenance need under JDIS scheme. For instance, if a part failure occurs or is predicted to occur, JDIS initiates a series of actions that can provide the right information for the engineer about the replacement of parts at the right time. This way, human interaction is minimized as data flows from the aircraft through the maintenance infrastructure and ultimately to the supplier community.

General Motors' research labs are using predictive equations for calculating remaining oil based on monitoring engine usage over time [34]. Engine oil breaks down as a function of time at temperature oxidation and engine usage related contamination.

On selected vehicles this algorithm is programmed into the engine control modules (ECM) and keeps the driver aware of their oil life status and displays via the vehicle's driver information center (DIC) display.

2 LIFE CONSUMPTION MONITORING METHODOLOGY FOR ELECTRONICS

Life consumption monitoring (LCM) is a health monitoring method to assess product's reliability based on its remaining life in a given life cycle environment. The life consumption monitoring process involves continuous or periodic measurement, sensing, recording, and interpretation of physical parameters associated with a system's life cycle environment to quantify the amount of system degradation. This section explains a life consumption monitoring methodology for electronics.

Life consumption monitoring methodology has six steps to estimate the remaining life of an electronic product (Figure 2.1). These steps include failure modes, mechanisms and effect analysis (FMMEA), virtual reliability assessment, monitoring of the critical parameters of the product's life cycle environment, simplification of the monitored data, stress and damage accumulation analysis, and remaining life estimation. Each step will be described in this section.

The life consumption monitoring methodology described in this thesis is an improvement over the existing methodology developed by Ramakrishnan et al. [35] for his Masters thesis. The existing methodology focused on estimation of accumulated damage of solder joints for electronics. An assumption was made that temperature and vibration are the dominant environmental parameters that can cause failure due to solder joint fatigue.

The improved methodology has been extended and generalized to system level, where there is a possibility of various other failure mechanisms. Failure modes, mechanisms, and effects analysis (FMMEA) and virtual reliability assessment has been

included in the improved methodology to determine the dominant failure mechanism in a given life cycle environment and the corresponding environmental and operational parameters. Another step has been added to determine the remaining life of the product based on the accumulated damage information.

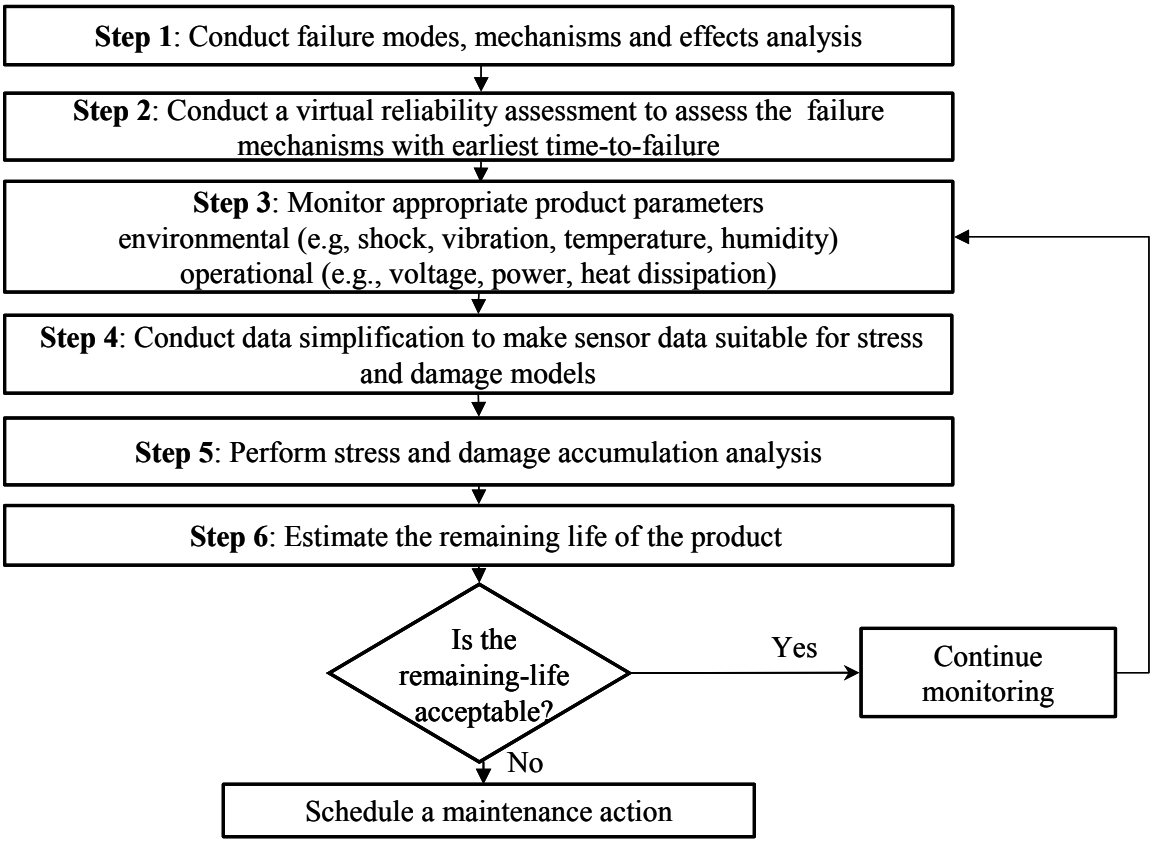

Figure 2.1: Various steps in the life consumption monitoring approach

2.1 Failure Modes, Mechanisms and Effects Analysis

An electronic product is typically a combination of components and interconnects, all having various failure mechanism by which they can fail in the life cycle applications. The objective of the failure modes, mechanisms, and effects analysis (FMMEA) in life consumption monitoring is to identify the failure mechanisms that can precipitate a

failure mode in the given environmental and operational conditions. Following sections discuss about the steps involved in FMMEA.

2.1.1 Identification of Failure Modes and Corresponding Failure Sites

The failure modes, mechanisms, and effects analysis (FMMEA) starts with identification of all possible failure modes and the corresponding failure sites. A failure mode is defined by how a failure is observed. Hence it is closely related to the functional and performance requirements of the product. Failure modes are identified by determining what could possibly go wrong or how a product can fail to meet its specifications. Typical failure modes for electronic products include electrical opens or shorts, change in resistance, intermittent resistance change. Failure site defines the location of failure, e.g., printed circuit board, plated through holes (PTH), components, interconnects.

2.1.2 Identification of Failure Mechanisms and Models

The second step in FMMEA is to determine all possible failure mechanisms followed by identification of corresponding failure models available. Failure models are used to identify the environmental and operational parameters along with the product geometry responsible for a specific failure mechanism. More details about various failure models for electronic components and printed circuit boards can be found in literature [36]-[41].

2.1.3 Identification of the Life Cycle Conditions

This step requires determination of the life cycle environment conditions for the product. The life cycle environment of a product consists of the assembly, storage,

handling, and usage conditions of the product, including the severity and duration of these conditions. Information on product usage conditions can be obtained from environmental handbooks or data monitored in similar environments. Some times it may be necessary to include the assembly, storage, handling and transportation conditions. The life cycle conditions are compared with the inputs to the failure models in the next step.

2.1.4 Selection of failure mechanisms that can precipitate a failure mode

Depending on the life cycle environment, particular failure mechanisms have the potential to cause product failure. This step eliminates some of the failure mechanisms based on inputs to failure models, life cycle environment conditions and product geometry. For example, metallization corrosion models require high moisture content to precipitate a failure mode. Hence if the moisture content is very low in a given environment, failure due to metallization corrosion might be eliminated. The failure mechanisms that cannot be eliminated are selected for analysis using virtual reliability assessment.

2.2 Virtual Reliability Assessment

Virtual reliability assessment method is used to assess potential failure mechanisms identified by the failure modes, mechanisms, and effects analysis (FMMEA). The objective of this step to identify the dominant failure mechanisms and corresponding environmental and operational parameters based on time-to-failures and identify the environmental and operational parameters for monitoring.

2.2.1 Prioritization of the Failure Mechanisms Based on Time-to-failures

This step starts with estimation of time-to-failures based on the failure mechanisms and models selected by FMMEA. The failure mechanisms are then ranked based on the time-to-failures. Failure models typically require product geometry along with life cycle environmental and operational parameters. At this stage of life consumption monitoring the product geometry is available Life cycle environment conditions for the analysis are taken from the sources identified during FMMEA. In cases of new products, environmental handbooks are good sources of information.

2.2.2 Identification of The Dominant Failure Mechanisms

This step identifies the dominant failure mechanisms based on the time-to-failure rankings. In principle, for a non-repairable unit the dominant failure mechanism is the one by which the first failure is expected to occur. But in practice, more than one dominant failure mechanism may need to be considered because of variability in materials, manufacturing processes, and life cycle loads. Failure mechanisms with time-to-failures less than the product life expectation are considered as candidate dominant failure mechanisms. In other words, failure mechanisms with time-to-failure greater than (20%, based on rule of thumb) the expected product life need not be considered. If maintenance is available until end of product life expectation, all failure mechanisms with time-to-failures below the product life expectation are considered as dominant failure mechanisms. While choosing dominant failure mechanisms for complex systems, tradeoff may be made based on cost, memory and processing capabilities.

2.3 Monitoring Appropriate Product Parameters

Monitoring product parameters involve measurement and monitoring of product life cycle environment, which includes the environmental and operational parameters identified by virtual reliability assessment. The life cycle environment of a product consists of the assembly, storage, handling, and usage conditions of the product, including the severity and duration of these conditions [2]. Specific life cycle loads on an electronic product include environmental conditions such as temperature, humidity, pressure, vibration or shock, radiation, contaminants, and loads due to electrical operating conditions, such as current, power and heat dissipation. These loads can affect the reliability of the product either individually or in combination with each other. Product parameters can be monitored in a continuous or periodic manner using various sensors mounted on or within the product. An ideal sensing device should be:

- Compatible with existing electronics (i.e., it should have minimal impact on the total cost, performance, and reliability of the existing product)
- Accurate, have low response time, and self-correcting (e.g., having temperature compensation) in operation
- Small, lightweight, and consuming system-independent and little power (preferably self-powered)
- Easy to incorporate into the system
- Easily accessible for data acquisition, service, maintenance, and upgrades

Typical sensors include temperature sensors (thermocouples, thermistors, and resistance thermo detector (RTD) sensors), humidity sensors, accelerometers, pressure sensors (piezoelectric, MEMS) etc. The data measured by these sensors are recorded by a

data logger for further processing. The recording process needs specification of parameters including sampling intervals for measurements, signal trigger values[1].

2.4 Data Simplification Processes

Data simplification is the process of converting the raw sensor data into a form suitable for the stress and damage models. Simplification of data is necessary since the monitored data cannot be directly used with the stress and damage models in many cases. For example, Engelmaier's model for thermal fatigue of solder joints requires temperature data in the form of temperature cycles and hence there is a need to convert the temperature data from sensors to equivalent temperature cycles. The data simplification process typically depends on the input requirements of the stress and damage assessment model. Some examples of data simplification include

- Conversion of irregular temperature history into a regular sequence of peaks and valleys for thermal fatigue analysis.
- Conversion of temperature reversals into relevant temperature cycle information.
- Conversion of acceleration data in time domain to power spectral density (PSD) in frequency domain.

Data simplification process can also provide data reduction if necessary. A suitable data reduction scheme is useful for analyzing large amounts of data by gain in computing speed and reduction in memory requirements.

[1] Some times data is recorded only if the value is more than a certain pre specified value. The pre specified value is known as signal trigger value.

2.5 Stress and Damage Accumulation Analysis

Stress and damage accumulation analysis is used to estimate the accumulated damage in the product based on simplified data. This step begins by creating numerical models based on product geometry and material properties. For example, creation of model for a circuit card assembly requires information on board material and dimensions, component material, dimensions, and their respective orientations. Information on product geometry is obtained from design specifications and manufacturer data sheets. The numerical model is used to estimate the stress at individual failure sites based on life cycle environment loads.

Based on the estimated stress values, the accumulated damage for the product in its life cycle environment is estimated. Estimation of accumulated damage involves two separate steps: 1) application of stress and damage models, 2) application of a suitable damage accumulation theory.

2.5.1 Stress and Damage Models

The purpose of stress and damage models is to determine or predict the occurrence of a specific wear out failure mechanism in a specific application. The prediction process looks at each individual failure mechanism (such as solder joint fatigue, electromigration, conductive filament formation, die cracking to name a few) to estimate the probability of failure. This approach can be applied to electronic parts used in military, space, telecommunication, industrial, automotive, aviation, and consumer utilization applications, and is applicable to the entire life cycle of the product.

Selecting the proper damage model is the key to the accuracy of the stress and damage accumulation analysis. Specific models for each individual failure mechanism

are available from a variety of reference books. These models can either be in the time domain or in the frequency domain. Stress and damage models can be divided into two major classes depending on the input requirements, i.e., models requiring cyclic inputs and models requiring non-cyclic inputs.

Models requiring cyclic inputs are typically used to determine the fatigue life or damage for a part. Examples of this class of models include Coffin-Manson's model for cyclic fatigue, Suhir's model for die fracture, and Pecht and Lall's model for wire fatigue. The following equation shows Coffin-Manson's model for thermal fatigue of solder joints.

$$N_F = \frac{1}{2}\left(\frac{\Delta\varepsilon}{2\varepsilon'_f}\right)^{\frac{1}{c}} \qquad (2.1)$$

where N_F is the number of cycles to failure, $\Delta\varepsilon$ is the cyclic strain, and c, ε'_f are material constants. A cycle is identified "when a material remembers its prior deformation history and changes its tangent stiffness to follow the original loading path". Since the data measured by a sensor is typically in the time domain (or in the frequency domain for vibration sensors), cycle counting methods are used to transform the original history into an equivalent cyclic history that can be directly incorporated into a fatigue damage model.

Models requiring non-cyclic inputs usually require time varying value of the independent variable as an input. Examples of this class of models include Black's model for electromigration, Kidson's model for intermetallic formation, and Howard's model for metallization corrosion. The following equation shows Black's model for electromigration.

$$t_F = Aj^{-2}e^{\frac{E_m}{kT}} \qquad (2.2)$$

where t_F is the time to failure, j is the current density (the time varying independent variable), T is the absolute temperature and A, E_m, k are constants.

2.5.2 Damage Accumulation Theories

Failures can be classified in two types – overstress and wear out. Overstress failures are catastrophic failures occurring due to single occurrence of a stress event that can exceed the intrinsic strength of the material. On the other hand, failures due to gradual accumulation of damage beyond the endurance limit of the material are known as wear out mechanisms. In well-designed and high-quality hardware, the accumulated damage should not exceed the damage threshold within the usage life of the product. Failure models describing wear out failures are usually based on values of environmental or operational variables.

Damage is defined as the extent of a system's degradation or deviation from a defect-free normal operating state. The basic postulate adopted by most fatigue engineers is that operation at a given cyclic stress amplitude will produce fatigue damage in a certain number of operation cycles. It is further postulated that the damage incurred is permanent, and operation at several different stress amplitudes in sequence will result in an accumulated damage equal to the sum of the damage accrued at each individual stress level. When the total accumulated damage reaches a threshold level, fatigue failure occurs. Many different damage models have been proposed to quantify damage caused by operation at varying stress levels. The Palmgren-Miner cumulative damage theory or the linear damage theory is the most common among these theories because of its

simplicity. This damage theory was proposed by Palmgren in 1924 and later developed by Miner in 1945 [42].

According to the classic S-N curve, operation at constant stress amplitude S produces complete damage in N cycles. Operation at the same stress amplitude (S) for number of cycles smaller than N, will produce a fractional damage. In the same way, operations over different stress levels S_i result in different damage fractions D_i. Failure is predicted to occur when the sum of the damage fractions equal or exceed unity, i.e.,

$$D_1 + D_2 + D_3 + \cdots\cdots + D_{i-1} + D_i \geq 1 \qquad (2.3)$$

The Palmgren-Miner hypothesis states that the damage fraction at any stress level S_i is linearly proportional to the ratio of the number of cycles of operation to the total number of cycles that would produce failure at that stress level, thus,

$$D_i = \frac{n_i}{N_i} \qquad (2.4)$$

Similarly, for damage models that estimate time-to-failure (e.g., Black's model for electromigration), damage is defined as

$$D_i = \frac{t_i}{TTF_i} \qquad (2.5)$$

where t_i is the time of operation and TTF_i is the time-to-failure estimated by the model.

The Palmgren-Miner hypothesis is the most widely used model in industry, mainly due to its simplicity. However the hypothesis does not recognize the influence of the order of application of various stress levels. Damage is assumed to accumulate at the same rate at a given stress level without regard to past history. In applying the Palmgren-

Miner rule to an irregular load history, care should be taken that cycles are defined in a rational manner.

2.6 Estimation of Remaining Life

Remaining life estimation is the process of estimating the remaining life of the product based on accumulated damage information. Sometimes, it is more useful to quantify product degradation in terms of physical parameters (e.g., time in days, distance in miles) than in terms of accumulated damage. Accumulated damage of the product is combined with product usage history to estimate the remaining life. This process assumes that there is no abnormality in product usage pattern in future. In other words, this step converts the accumulated damage in the electronic product into an equivalent amount of time that the product can continue to function before the start of wear out failures.

The remaining life estimation is updated regularly at the end of a pre selected time period. Hence the remaining life estimation process can take in to account any sudden change in the life cycle environment or usage of the product. The time interval between two updates is decided based on the product usage and its estimated lifetime based on virtual reliability analysis. Sometimes the safety level associated with the product can play an important role in determining the time interval.

2.7 Acceptable Remaining Life

The life consumption monitoring methodology described above concludes with an estimation of the useful remaining life of the product. At this point, the user is required to decide whether to keep the product in operation and continue monitoring or to abandon the mission and schedule a maintenance action. The choice of acceptable amount of remaining life depends on a variety of factors, such as the user's application and the

safety level associated with it. For example, if the application is known to be fairly reliable with multiple redundancies, a higher limit of acceptable remaining life may be chosen but if the application involves human participation or may compromise the safety of personnel, a lower acceptable limit of remaining life may is required.

3 EXPERIMENTAL CASE STUDIES ON LIFE CONSUMPTION MONITORING

The life consumption monitoring methodology described in chapter 2 was demonstrated in a real-time environment through two case studies. The life cycle environment for the case studies was chosen to be the underhood of an automobile. The case studies involved the following steps:

1. Mounting test boards under the hood of a car (1997 Toyota 4Runner) (Figure 3.1)
2. Conducting failure modes and effects analysis (FMEA) and virtual reliability assessment to determine and assess the dominant failure mechanisms and the corresponding environmental parameters.
3. Monitoring the underhood thermal, shock and vibration environment of the test board in the car.
4. Simplifying the monitored environment and performing a physics-of-failure-based reliability analysis to estimate the life consumption for the test board.
5. Monitoring resistance of the solder joints in real time to find out the actual life.
6. Comparing the estimated and the actual life results.

The test board was a FR-4 printed circuit board (PCB) consisting of eight surface mount leadless inductors manufactured by ACI AppliCAD Inc. The inductors were soldered to the PCB with Pb-Sn eutectic solder. The board was bolted at its two corners to an aluminum bracket, which made the board act like a cantilever to vibrations[2].

[2] Cantilever mounting was designed in order to accelerate the effect of road vibration and was not planned

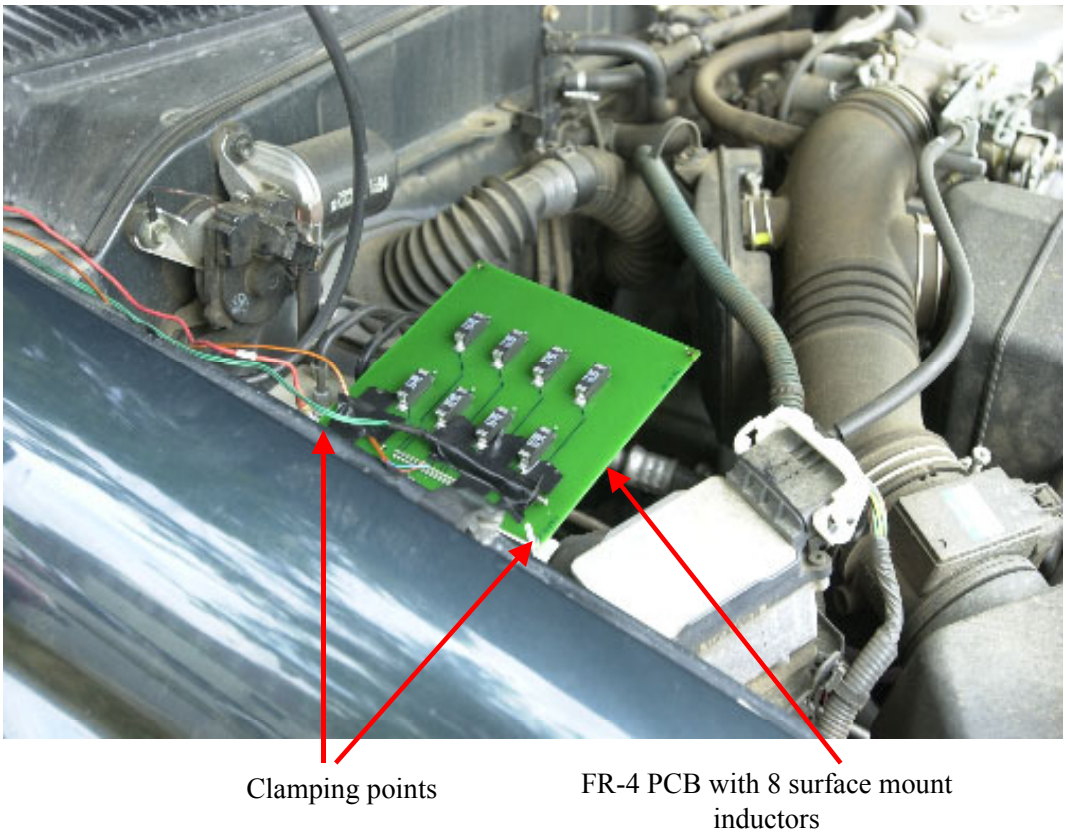

Figure 3.1: Experimental setup with the test board mounted under-the-hood of a car (1997 Toyota 4Runner).

3.1 Failure Modes, Mechanisms and Effects Analysis

Failure modes, mechanisms, and effects analysis (FMMEA) was conducted for the test board assembly to assess all possible failure modes and mechanisms in the automobile underhood environment. Environmental and operational parameters of interest were identified based on inputs to the available failure models. When a failure model is not available for a particular failure mechanism, environmental and operational parameters were identified based on prior experience and literature. Identified

---

to be representative of time-to-failure in automobile electronic modules.

environmental and operational requirements were compared with the existing loading conditions in the underhood environment to determine the potential failure mechanisms. The potential failure mechanisms were used for analysis by virtual reliability assessment. Table 3.1 shows the failure modes, mechanisms, and effects analysis for the circuit card assembly. Plated through hole (PTH) fatigue, conductive filament formation (CFF), electromigration, metallization corrosion, and solder joint fatigue were identified as the potential failure mechanisms by this analysis.

3.2 Virtual Reliability Assessment

Virtual reliability assessment was conducted to assess the time-to-failure using the failure mechanisms and models identified by failure modes, mechanisms, and effects analysis (FMMEA) including plated through hole fatigue, conductive filament formation, electromigration, metallization corrosion, and solder joint fatigue. Information about product dimensions and geometry were obtained from design specification, board layout drawing and component manufacturer data sheets. Environmental data for analysis including temperature, vibration and humidity were obtained from the Society of Automotive Engineers (SAE) environmental handbook and Washington DC area weather reports. Figure 3.2 shows the average power spectral density (PSD) plot for the vibration on a car frame from SAE handbook [43]. The car was assumed to run average 3 hours per day. Table 3.2 shows the temperature data used for defining the underhood environment. The maximum relative humidity for the underhood environment was 98 % at 38 ^{o}C [43]. Humidity conditions were used to estimate time-to-failure for corrosion and conductive filament formation.

Table 3.1: Failure Modes and Effects Analysis (FMEA) for the circuit card assembly used for the experiment.

Item name/ failure site	Failure mode	Failure effect	Failure mechanism	Failure model	Cause of failure	Comments
Printed circuit board (PCB)	Electrical open in PTH	Change in resistance of PCB assembly	PTH fatigue	CALCE PTH barrel thermal fatigue model	Temperature cycling	Virtual reliability assessment required
	Electrical short between PTHs	No current flow through components	Conductive filament formation (CFF)	Rudra and Pecht model	Voltage, high RH, and tighter PTH spacing	Virtual reliability assessment required
	Electrical short/ open, change in resistance in the metallization traces	Change in resistance of PCB assembly	Electro-migration	Black's model	High current density and temperature	Virtual reliability assessment required
			Corrosion in metallization traces	Howard's model	High RH, electrical bias, ionic contamination	Virtual reliability assessment required
		Open	EOS/ ESD	No model available for EOS/ ESD of board metallization traces	Discharge of high potential through dielectric material	Too high conductor spacing (in the order of centimeters) to cause EOS/ESD
	Fracture in the PCB	Crack/ breaking of PCB	Buckling	Overstress failure dependent on critical load	Compressive loads on the PCB	No compressive loads applied to the PCB

Item name/ failure site	Failure mode	Failure effect	Failure mechanism	Failure model	Cause of failure	Comments
Components (Inductors)	Short between windings	Change in inductance of PCB assembly	Wearout of winding insulation	No model available for Inductors	Overheating due to excessive current and prolonged use at high temperature	Maximum operating temperature is low compared to rated temperature of the inductors (125 C). Current passing through the inductors (~50 mA) is much below the maximum rated current (9 Amps)
	Short between windings and the core	Change in resistance of PCB assembly	Wearout of winding insulation	No model available for Inductors	Overheating due to excessive current and prolonged use at high temperatures	
	Open circuit inside the inductor	No current flow through PCB assembly	Breaking of winding	No model available for Inductors	Prolonged use at high temperatures	
Solder joints	Intermittent change in electrical resistance	Intermittent malfunctioning of PCB assembly	Solder joint fatigue	Engelmaier's thermal fatigue/ Steinberg's vibration	Temperature cycling and vibration	Virtual reliability assessment required

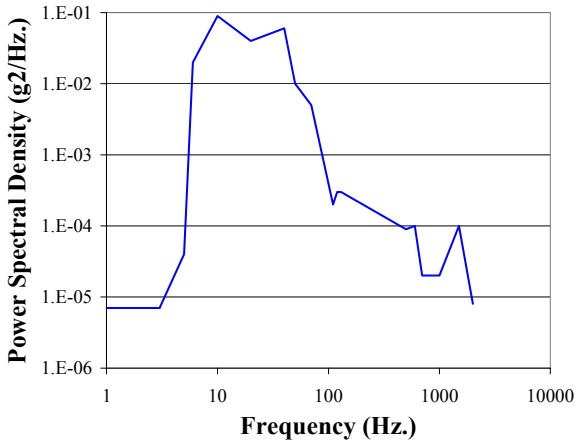

Figure 3.2: The power spectral density plot used for the virtual reliability assessment

Table 3.2: Data used for defining the temperature environment for the virtual reliability assessment

Maximum under hood temperature (near the frame)	121 ^{o}C
Average daily maximum temperature [44]	27 ^{o}C
Average daily minimum temperature [44]	16 ^{o}C

Table 3.3 shows the time-to-failures for different failure mechanisms obtained from virtual reliability assessment. It is clear from the table that solder joint fatigue is the dominant mechanism in the given life cycle environment. The environmental factors that can cause solder joint fatigue were found to include temperature cycling and vibration. The virtual reliability assessment predicted. Virtual reliability assessment predicted 34 days to failure based on solder joint fatigue.

Table 3.3: Virtual reliability assessment

Failure mechanism	Failure model	Time-to-failure	Probability of failure
Plated through hole (PTH) fatigue	CALCE PTH barrel thermal fatigue model (calcePWA)	> 10 years	Low
Conductive filament formation (CFF)	Rudra and Pecht model (calceFAST)	4.6 years	Low
Electromigration	Black's model (calceFAST)	>10 years	Low
Corrosion in board metallization traces	Howard's model	1 year[3]	Low
Solder joint fatigue	Engelmaier's thermal fatigue and Steinberg's vibration model (calcePWA)	34 days	High

A monitoring and data simplification schemes were developed for monitoring and analyzing the automobile underhood environment for solder joint fatigue analysis. The electrical indications of failure in case of solder joint fatigue are characteristically intermittent because the fractured solder joint surfaces do not separate physically as long as the component is attached to the substrate by other solder joints [45]. For the case study, product malfunction was monitored through intermittent change in resistances, which is consistent with characteristics of solder joint failure.

[3] Time-to-failure was obtained in the worst case conditions with the presence of an electrolyte. The actual time-to-failure will be much higher than one year.

3.3 Monitoring Product Parameters

A battery powered data logging device equipped with an internal tri-axial accelerometer and an integrated temperature and humidity sensor (Figure 3.3) was used to record the shock, vibration and temperature environment of the test board assembly at programmed intervals [46]. The data logger is capable of recording both static and dynamic type of data. Static data can be completely characterized by a single reading, where as dynamic data varies rapidly with time. In addition to integrated sensors, the data logger also provides extra static and dynamic channels for connection to external sensors. For the experiment temperature was monitored as static data and vibration was monitored as dynamic data. The recorder's memory (8 MB) was divided into two partitions:

- Time-triggered: This allows the user to specify the minimum time interval to elapse before recording begins. This feature is primarily for measuring static data.
- Signal-triggered: This allows the user to specify the minimum value of a parameter (i.e., signal trigger) that should be exceeded before the recording begins. An event is defined when the measured parameter exceeds the signal trigger value and a predefined number of samples are recorded. This feature is primarily for measuring dynamic data.

For the experimental set up, the data logger was programmed in such a way that it required the specification of the following parameters:

- Time interval between temperature measurements
- Sampling rate for shock and vibration (i.e., the number of samples counted per second)
- Sample size for shock and vibration (i.e., the number of samples per event)

- Signal trigger values
- Filter frequency for vibration

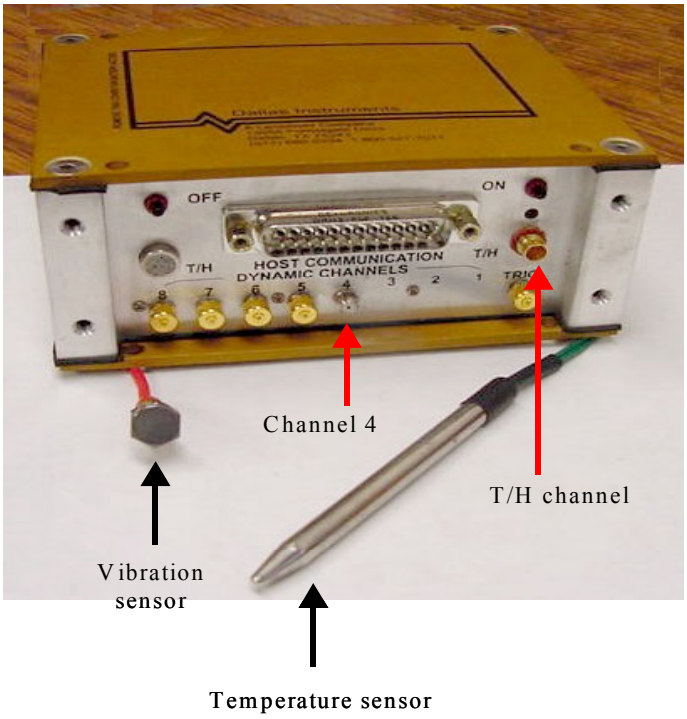

Figure 3.3: The data logger with external temperature and vibration sensor

The data recorder could not be placed directly under the hood of a car because its internal sensors had a maximum rated temperature of 55 °C. Further its size and weight precluded its installation anywhere under-the-hood. Hence external temperature and vibration sensors were used for monitoring the underhood environment.

An external RTD (resistance thermo-detector) temperature sensor was taped on the test board with the help of high temperature resistant tape to monitor the temperature. The sampling interval for temperature measurement was chosen to be one minute so that the data recording device can capture even quick temperature changes arising due to starting of the engine.

A piezoelectric accelerometer was mounted on one of the clamping points of the test board to monitor vibration input. The vibration of the circuit card assembly for this experimental setup was mainly due to the road and driving condition and hence could be categorized as random vibration. A random vibration signal typically consists of several frequencies. The range of frequencies that can be accurately monitored is dependent on the chosen sampling scheme (i.e., sample rate, sample size, filter frequency).

3.3.1 Sampling Issues for Monitoring of Continuous Signals

Most signals behave as continuous phenomena over their period of acquisition, and provide a history of the parameter being measured as a function of time. Sampling is the process of obtaining a series of discrete numerical values from a continuous function. There are electronic circuits associated with sensors that observe an instantaneous source signal at regular intervals and convert it into an electrical signal with a numerical value analogous to the source signal.

Signals are made suitable for digital processing by converting their sampled value into an equivalent numerical value by an analog-to-digital converter. Each value is represented by a finite number of on/off states of electronic elements. The converter has an input-output relationship, which is a series of steps. The size of the steps depends on the total range to be covered and the number of steps available.

The most important consideration in sampling is the selection of the sampling interval. Sampling points that are too close together will yield redundant data, while sampling points that are too far apart will lead to confusion between the low and high frequency components of the signal. For example, consider the time record shown in Figure 3.4. Let the record be sampled such that the time interval between adjacent

sampling points is h seconds. The sampling rate is hence 1/h samples per second. Since at least two sample points are required to define a cycle of given frequency (i.e., one point each for the start and the end of a cycle), the number of cycles per second (or the frequency of sampling) is 1/2h. Thus, the highest frequency component that can be defined by sampling at the rate of 1/h samples per second is 1/2h. This cutoff frequency f_C (equal to 1/2h) is called the "Nyquist frequency", and the corresponding time between samples h is called the "Nyquist interval".

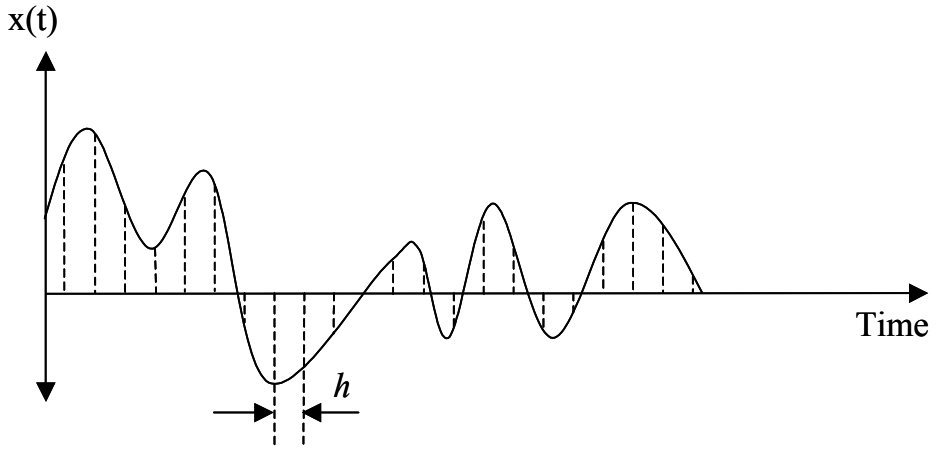

Figure 3.4: Sampling of a continuous time record

Any frequency f above f_C contained in the signal will be superimposed or "folded" back into the frequency range from 0 to f_C and be confused with data in the low-frequency range. This problem, which is called aliasing, is a potential source of error in sampling. For any frequency f in the range $0 \le f \le f_C$, the frequencies that will be aliased with f are $2nf_C \pm f$, where n is a natural number from 1 to N. To prove this, consider a sampling interval $t = 1/2f_C$. Then,

$$\cos 2\pi(2nf_C \pm f)t = \cos 2\pi(2nf_C \pm f)\frac{1}{2f_C} = \cos\left(2n\pi \pm \frac{2\pi f}{2f_C}\right) = \cos 2\pi f \frac{1}{2f_C} = \cos 2\pi ft \qquad (3.1)$$

Thus, all data at frequencies ($2nf_C \pm f$) have the same cosine function amplitude as the data at frequency f when sampled at times $1/2f_C$ apart, and hence all data at the higher frequencies will be aliased (or superimposed) on data at frequency f. For example, data at frequencies 170 Hz, 230 Hz, 370 Hz, 430 Hz, and so on will be aliased with data at 30 Hz if f_C = 100 Hz. Hence, the sampling interval *h* should be carefully chosen to prevent aliasing.

Two methods are available to prevent aliasing: 1) to choose *h* sufficiently small so that it is physically unreasonable for data to exist beyond the cutoff frequency f_C or 2) to filter the original data prior to sampling so that information beyond a maximum frequency is no longer contained in the filtered data. The second method, which involves the use of a low-pass filter circuit that only allows passage of frequencies below the frequency of the filter, is often preferred over the first method to save on computing time and costs [47]. Hence a low-pass filter was used in this thesis to screen out all frequencies above the Nyquist frequency to prevent aliasing.

In order to select the vibration analysis range, the data recorder was first programmed to collect data at its maximum sampling rate[4], and the resulting frequency spectrum was analyzed. It was observed that the power spectral density (PSD) of the vibrations was concentrated below 400 Hz and the PSD was negligible above 600 Hz (below 10^{-6} g^2/Hz.). Hence, the frequency analysis range was conservatively selected to be 1 to 700 Hz. Accordingly the sampling rate and sample size were selected to be 1800

[4] This was done to find the frequency range of interest and to ensure that any high-frequency vibrations would not be eliminated in the actual experiment.

samples/second and 1024 samples. The anti-alising filter frequency was chosen to be 700 Hz.

3.4 Data Simplification

Almost all monitoring systems use sensors to measure various loads present in a product's life cycle environment. Sensors mounted either near or within the product to be monitored provide electrical output signal in response to a specified measurand. Most signals from sensors behave as continuous phenomena over their period of acquisition, and provide a time history of the parameter being measured. This data in time domain cannot be directly used with the physics-of-failure models. This section describes the method to make temperature and vibration data compatible to the physics-of-failure models.

3.4.1 Temperature Data Simplification

Temperature based damage estimation models require temperature data in terms of cycles. The physics-of-failure definition of cycles includes the maximum, minimum temperature, ramp times and dwell times at maximum and minimum. Rainflow cycle counting algorithms are usually used to identify the cycles based on a given loading profile [48]. The temperature based reliability assessment models require cycle information that includes cycle maximum, minimum temperature, dwell and ramp times. The 3-parameter rainflow cycle counting method can identify cycles in a manner consistent with the PoF definition of cycles [49], [50]. The input to the 3-parameter rainflow cycle counting algorithm is a time history consisting of several reversals [5].

[5] A reversal is defined as a point where the first derivative changes its sign, i. e., a peak or a valley.

3.4.1.1 Ordered Overall Range (OOR) method

The data is first converted to a sequence of reversals using the ordered overall range (OOR) method. The OOR method allows the user to convert an irregular history in time domain into a regular sequence of peaks and valleys. The OOR method can be described as follows [51]

- The largest peak [6] of the temperature history is selected as the first candidate
- The next valley that differs from the largest peak by more than a cut off level is selected as the tentative candidate.
- The cut off level is defined as a fraction of the difference between the largest peak and the lowest valley. The fraction is known as the reversal elimination index (s).
- Peaks are checked to see if they differ from the new candidate by more than the screening level (event 'x'), and valleys are checked to see if they are lower than the candidate (event 'y'). If event 'y' occurs first (i.e., before event 'x'), then the candidate is rejected and the new valley becomes a candidate. If event 'x' occurs first, the candidate is validated and the newly found peak becomes the next candidate.
- The next peak that differs from the new candidate by more than a cut off level is selected as the tentative candidate.
- Valleys are checked to see if they differ from the candidate by more than the screening level (event 'x'), and peaks are checked to see if they are higher than the candidate (event 'y'). If event 'y' occurs first (before event 'x'), then the candidate is

[6] The algorithm requires selection of either of the extreme reversals in the history (either the largest peak or the smallest valley) as the first candidate. In this article the algorithm is explained taking the largest peak as the first candidate.

rejected and the new peak becomes a candidate. If event 'x' occurs first, the candidate is validated and the newly found valley becomes the next candidate.

- This process continues until the last reversal is counted.
- Since the counting process starts from the largest peak (which may not be the first reversal in the history), the method has to be applied to both sides of the starting reversal to take the entire load history into account.

When the reversal elimination index is equal to zero, all the reversals in the load sequence are preserved. The OOR algorithm has the capability of eliminating some of the temperature reversals, which are potentially less damaging, there by achieving data reduction. Data reduction can be achieved by specifying a non-zero reversal elimination index. Figure 3.5 explains the underlying concept of the OOR algorithm pictorially. In the figure, the highlighted points are selected only if $l \geq s \times L$.

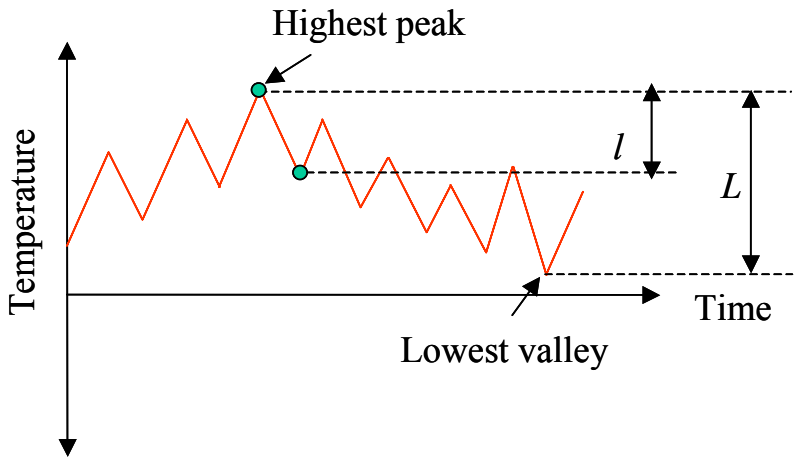

Figure 3.5: Temperature history showing the reversals (i.e., peaks and valleys)

3.4.1.2 Cycle Counting

Cycle counting methods [48] are used to transform a time history consisting of several reversals (peaks and valleys) into an equivalent cyclic history. Cycle counting methods are used when a fatigue analysis needs to be performed.

The physical interpretation of a cycle is a condition when the applied load returns the material to the state it was before the load excursion occurred. If the applied load is of a mechanical nature (such as force or torque), the material forms a closed stress-strain hysteresis loop when this condition is satisfied. For a repeatedly applied load history, the following two rules apply:

- When the load reaches a value at which loading was previously in the reverse direction, a stress-strain hysteresis loop is closed, defining a cycle. The stress-strain path beyond this point is the same as if the loading had not been reversed.
- Once a load sequence forms a closed loop, this sequence does not affect the subsequent behavior.

For the load history shown in Figure 3.6, the first rule is invoked at points 2', 7', 5', and 1'. The first rule is also satisfied just beyond 5', where the load reaches the same value it had at point 3. But the second rule also applies, and since excursion 2-3-2' has already formed a cycle, there is no additional closed cycle.

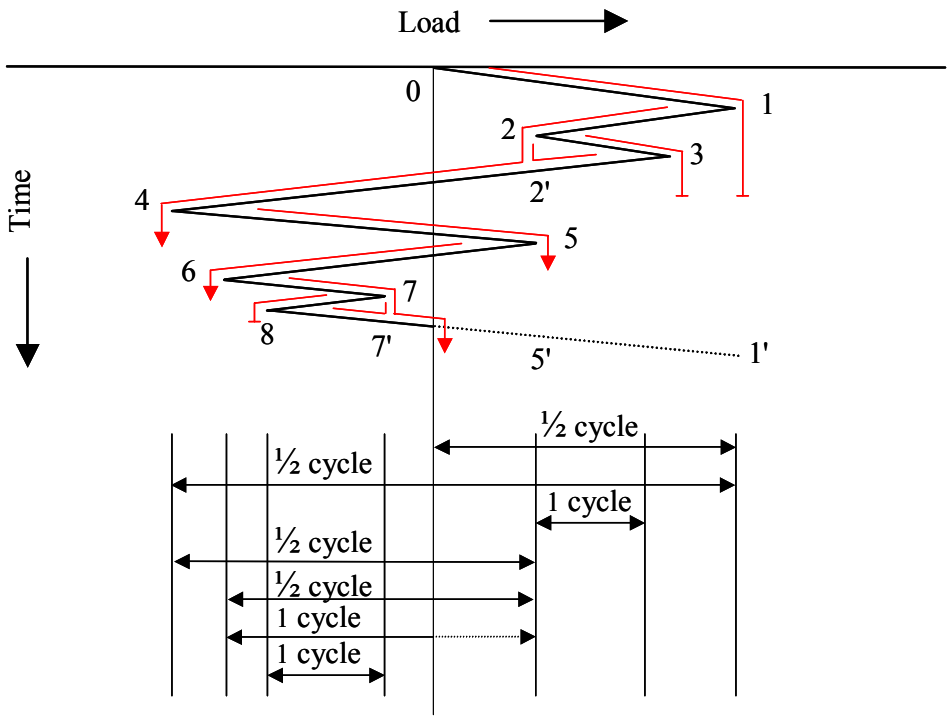

Figure 3.6: Identifying cycles in a load history

For non-repeating and open-ended load histories, the rules stated above are incomplete if the absolute value of the load at any point during the history exceeds its value at the first peak. Of the various cycle counting methods available (peak counting, simple range counting, peak-between mean counting, level crossing counting, fatigue meter counting, range-pair counting, and rainflow counting), only the rainflow and the range-pair counting methods are capable of handling this more general situation (of non-repeating histories). However, no damage is calculated for some parts of the original history if the range pair method is used, whereas the rainflow method accounts for every part of the history. Hence, the rainflow method was used in this thesis for counting cycles.

In the rainflow cycle counting method, the load-time history is plotted in such a way that the time axis is vertically downward, and the lines connecting the load peaks are imagined to be a series of sloping roofs. The rain flow is initiated by placing drops successively at the inside of each reversal. The method considers cycles as closed hysteresis loops formed during a history, which is consistent with the definition of a cycle described in the previous section. Following rules are applied on the rain dripping down the roofs to identify cycles and half cycles:

- The rain is allowed to flow on the roof and drip down to the next slope except that, if it initiates at a valley, it must be terminated when it comes opposite a valley equal to or more negative than the valley from which it initiated. For example, in Figure 3.7, the flow begins at valley 1 and stops opposite valley 9, valley 9 being more negative than valley 1. A half cycle is thus defined between valley 1 and peak 8.
- Similarly, if the rain flow is initiated at a peak, it must be terminated when it comes opposite a peak equal to or more positive than the peak from which it initiated. In Figure 3.7, the flow begins from peak 2 and stops opposite peak 4, peak 4 being more positive than peak 2. A half cycle is thus counted between peak 2 and valley 3.
- The rain flow must also stop if it meets rain from a roof above. In Figure 3.7, the flow beginning at valley 3 ends beneath peak 2. This ensures that every part of the load history is counted once and only once.
- Cycles are counted when a counted range can be paired with a subsequent range of equal magnitude in the opposite direction. If cycles are to be counted over the duration of a profile that is to be repeated block by block, cycle counting should be started by initiating the first raindrop either at the most negative valley or at the most

positive peak, and continuing until all cycles in one block are counted in sequence. This ensures that a complete cycle will be counted between the most positive peak and the most negative valley.

The simple rainflow method does not provide any information about the mean load or the cycle time. A modified method called 3-parameter rainflow cycle counting is used to handle this situation. This method accepts a sequence of successive differences between peak and valley values (P/V ranges) in the time history as an input, and determines the range of the cycle, the mean of the cycle, and the cycle time. The modified method identifies cycles as follows [50]: Consider three successive P/V differences d_1, d_2, and d_3, as shown in Figure 3.8. A cycle is identified only if the following condition is true:

$$d_1 > d_2 \leq d_3 \qquad (3.2)$$

The condition of the above equation is called the 'loop condition.' For a given sequence of P/V ranges, if the loop condition exists, the method picks the loop corresponding to size d_2 off the cycle, leaving only the residual wave 1-2-4-5, corresponding to a half-loop size (d_3-d_2+d_1) in the load plot. This operation is called 'loop-reaping.'

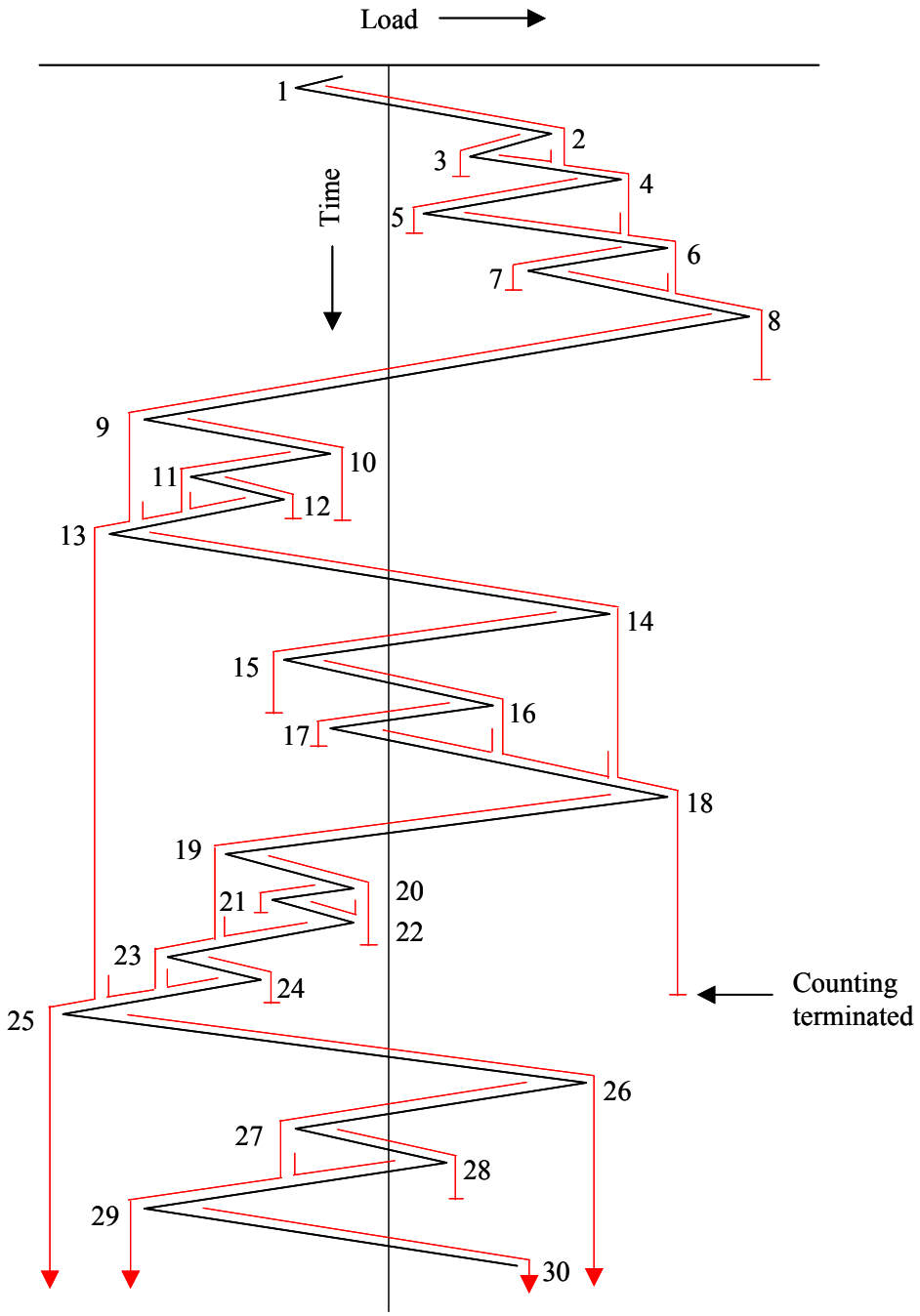

Figure 3.7: Rainflow cycle counting

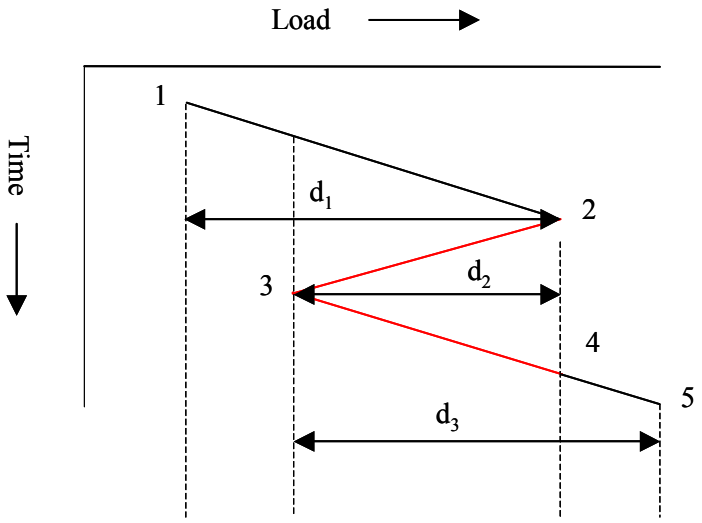

Figure 3.8: Loop condition and loop reaping operations

For a given sequence of P/V ranges, the 3-parameter rainflow method "reaps" the smaller cycles that occur during a larger cycle. The range, mean, and half-cycle time of the residual half cycle is adjusted according to the loop-reaping condition, and the process is applied until the last P/V range is read.

Solder joint fatigue models are based on total possible thermal expansion mismatch and creep at extreme temperature [45]. Stress relaxation in solder joints (viscoplastic materials) is a time dependent creep phenomenon and requires sufficient dwell time at the extreme temperature. However, once the stress relaxation is complete for a given cycle, there is no more damage in the solder joints due to creep in that cycle. The damage due to the total thermal expansion mismatch remains the same as long as the extreme temperatures are the same. Hence the data simplification algorithm should provide enough dwell time at the extreme temperatures for a conservative estimation. To account for this, the data simplification algorithm assumes one fourth of the half cycle

time at temperature extremes as the dwell time, where half cycle time is defined as the time for temperature transition from valley to peak or peak to valley [49].

3.4.2 Vibration Data Simplification

Vibration data is typically measured as acceleration with the help of accelerometers. In general the data collected from accelerometers represent random vibration (i.e., it cannot be described by an explicit mathematical relationship). The physics-of-failure based reliability assessment models require the random vibration data to be described in terms of its power spectral density (PSD). The PSD describes the frequency composition of the vibration in terms of its mean square value over a frequency range. Fourier Transform analysis is used to transform the acceleration data from time domain to the frequency domain, and vice versa. The result of the Fourier Transform analysis is usually a plot of amplitude/ power as a function of frequency. In real life collected data is sampled and not continuous. Hence Fast Fourier Transform (FFT) is employed to analyze discrete (or sampled) data. The power spectral density was calculated from the sampled data (i.e., the type of data recorded by the data logger) using the Cooley-Tukey method, which is based on fast fourier transform (FFT) of the original sampled acceleration data [47]. For a sequence of acceleration values h_k sampled over a record length T, the Cooley-Tukey method defines the PSD function at any frequency f as

$$G(f) = \frac{2h}{N}\left|X_k\right|^2 \qquad (3.3)$$

where X_k are the FFT components of the N sampled acceleration values of amplitude h_k averaged over the record length T. The expression for X_k is given by

$$X_k(n) = \sum_{k=0}^{N-1} h_k e^{i\frac{2\pi kN}{n}} \qquad (3.4)$$

where N is the sample size. The independent variable n can be related to the frequency by the relation $f_n = (n/Nh)$, where h is the sampling interval between adjacent points and T is the total record length.

For this thesis the acceleration data from the piezoelectric accelerometers were converted to respective PSD using the SAVER PSD analysis software [46].

3.5 Stress and Damage Accumulation Analysis

The objective of a physics-of-failure stress and damage accumulation analysis in life consumption monitoring is to determine the accumulated damage due to various failure mechanisms for the electronic product in the given environment.

For this thesis, the circuit card assembly was modeled in calcePWA[7] reliability assessment software. The software creates a finite element model of the circuit board assembly based on the various material properties, board dimension, component type, component dimensions and their respective orientations. Material properties for the model were taken from calcePWA material database[8]. Component dimensions were obtained from the respective part data sheet from Vishay Dale. Board dimensions and the component orientations were taken from the board layout drawing.

---

[7] calcePWA is a physics-of-failure based virtual reliability assessment tool for circuit card assemblies developed by CALCE Electronic Products and Systems Center, University of Maryland, College Park. The software makes use of numerical analysis and failure mechanisms) to estimate time-to-failure.

[8] calcePWA software has material property database for a number of materials commonly used in the electronic industry.

Once a model of the board is created, the software uses the environmental data to estimate the stress near each potential failure site (solder joint in this case) using the finite element model. For determining the stress under each solder joint it is important to provide the correct boundary condition to the software. The boundary conditions of the test board were defined as follows:

- Temperature on the test board was considered to be uniform with conduction and natural convection. This is a reasonable assumption as there is no power generation by the components.
- For vibration analysis two corners of the board were modeled as clamped supports.

Boundary conditions assumed for the vibration analysis were verified by comparing the experimentally evaluated natural frequencies of the board with the modeling results. The modeling predicted natural frequencies of the circuit card assembly as 25.7 Hz, 77.5 Hz, 145.4 Hz, and 274.8 Hz. To check this, another external accelerometer was mounted on the PCB. The ratio of the response of the PCB to the excitation given to the PCB at various frequencies was plotted against the frequency. Peaks of this plot give the experimental natural frequencies. Figure 3.9 shows that the natural frequencies occur at 19.3 Hz, 79.1 Hz, 149 Hz, and 262 Hz., which is in close agreement with the modeling prediction.

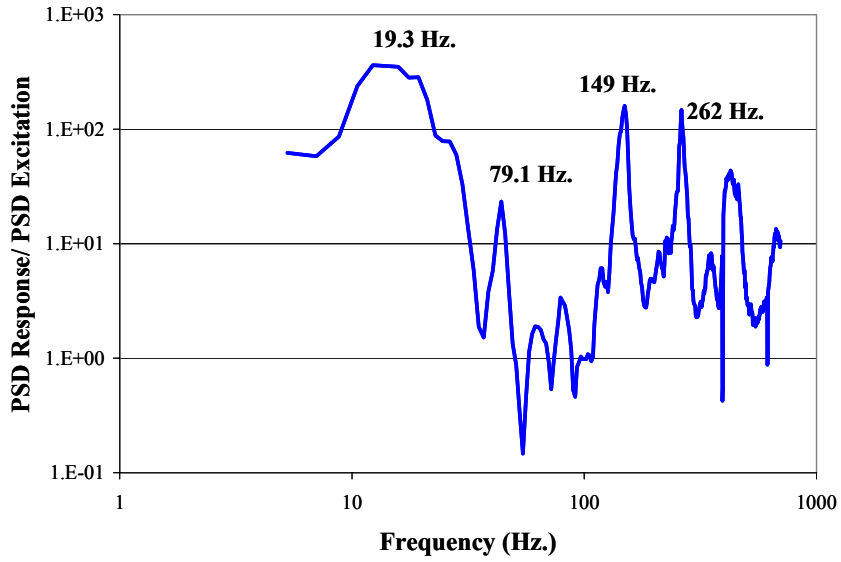

Figure 3.9: Ratio of the response of the PCB to the excitation vs. frequency. The peaks in this plot identify the natural frequencies.

The computed stress is then used to estimate the damage fraction based on physics-of-failure models for selected failure mechanisms. The basis of damage assessment is that operation of the product at a given stress amplitude will produce some amount of damage, the magnitude of which will be related to the total time of operation at that stress amplitude and the total time that would be required to produce failure of an undamaged part at that stress amplitude. When the total accumulated damage reaches a critical level, failure is predicted to occur. For this thesis, solder joint failure models for temperature cycling, shock and vibration were used to estimate the accumulated damage. The software used Engelmaier's first order model for thermal fatigue and Steinberg's equation for vibration induced fatigue on the solder joints. More details about the damage models can be found in the appendix.

3.6 Remaining Life Assessment

Remaining life estimation step calculates the useful life of the product (e.g., the time in days, distance in miles) through which the product can function reliably, based on the damage accumulation information. The remaining life was calculated on a daily basis by subtracting the life consumed on that day from the estimated remaining life on the previous day. This approach used an iterative formula to find out the remaining life [52].

$$RL_N = RL_{N-1} - D_N * TL_{N-1} \qquad (3.5)$$

where RL_N is the remaining life at the end of day N, TL_N is estimated total life at the end of day N and D_N is the damage ratio accumulated for day N.

3.7 Failure Definition and Detection

Solder joint failure due to fatigue is defined as the complete fracture through the cross section of the solder joint with solder joint parts having no adhesion to each other. A solder joint that fails fully by fracturing does not necessarily exhibit an electrical open or even a very noticeable increase in electrical resistance. Electrically, the solder joint failure manifests itself only during thermal and mechanical transients or disturbances in the form of short duration resistance spikes. The thermal and vibration fatigue models used for the analysis are also based on intermittent resistance spikes, i.e., interruption of electrical discontinuity for small periods of time (more than 1 μs) [45].

For the case studies in the thesis, the functional degradation of the circuit card assembly was monitored experimentally in terms of resistance change of the solder joints. An event detector circuit was connected in series with all the components and solder joints to indicate intermittent resistance increase. The event detector was connected to

the data logger to record the time when there was an increase in resistance. The intermittent increases in resistances were termed as "resistance spikes." Resistance spikes for the experiment were defined to be intermittent increase in resistance by 100 ohms for each solder joint [54], [55]. Failure was defined as occurrence of fifteen such resistance spikes.

The event detector circuit sends a continuous direct current signal through the daisy-chained circuit containing the inductors and the solder joints in series. Since the inductors offer zero resistance to the direct current, the resistance of the daisy-chained circuit is dependent on the resistance of the solder joints. The resistance offered to the direct current was compared with the preset value (100 ohms increase for each solder joint). The comparison results were logged at the end of every second. This time interval was limited by the capability of the data logger.

To determine change in resistance of the individual components and solder joints, the resistances were measured during the experiment on a regular basis with the car engine off.

3.8 Monitored Environment and Results

This section describes the monitored environmental parameters (e.g., temperature, shock and vibration) for the test board assembly for the case studies. The monitored data was simplified and used with the physics-of-failure models to estimate the remaining life of the test board assembly.

3.8.1 Case Study-I

The temperature sensor used for the case study was Kele's Model STR-91S two-wire strap-on RTD sensor with a temperature range up to 200 ^{o}C. A single axis

piezoelectric (Endevco's model 2226C) accelerometer was mounted on one of the clamping points of the test board to measure the out-of-plane acceleration for the board. Figure 3.1 shows the experimental setup for case study-I.

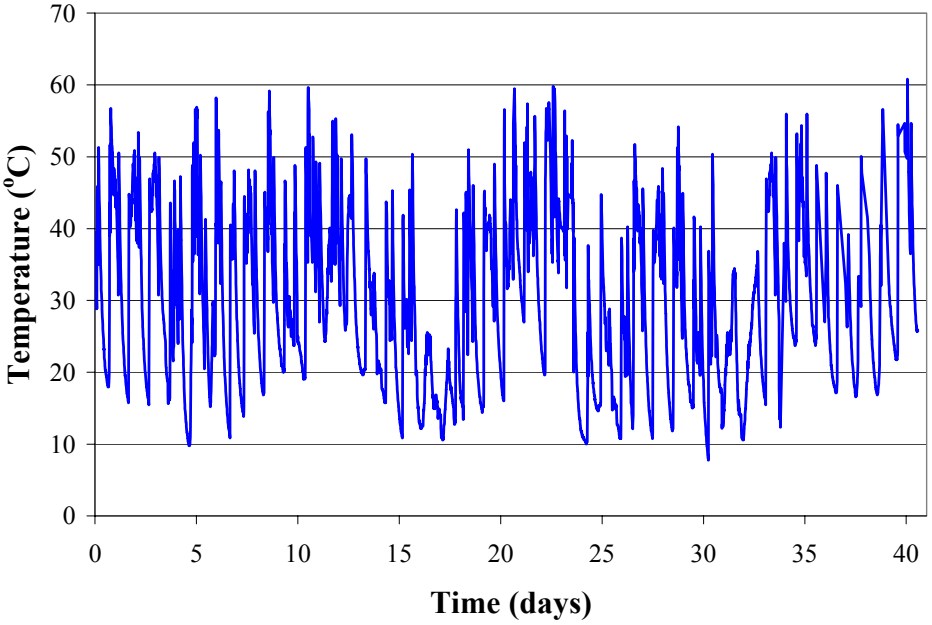

Figure 3.10: Monitored temperature during case study-I

The temperature on the test board in the underhood environment was monitored for a period of 42 days. Figure 3.10 shows the monitored temperature for the experiment period. Each data point is separated at an interval of one minute. The average temperature and the maximum temperature seen by the test board assembly during case study-I are 30 ^{o}C and 61 ^{o}C respectively.

The temperature vs. time history for 42 days was converted to an equivalent sequence of peaks and valleys (for thermal fatigue analysis) using the ordered overall range (OOR) method. For this analysis the reversal elimination index was chosen to be 0%, i.e., all the reversals were chosen as input to the cycle counting algorithm. Figure 3.11 shows the acquired temperature data converted to peaks and valleys. The sequence was converted to temperature cycles using the 3-parameter rainflow cycle counting method. 275 temperature cycles were identified for case study-I. The cycle information obtained from the rain flow cycle counting method was used as input to the calcePWA thermal module.

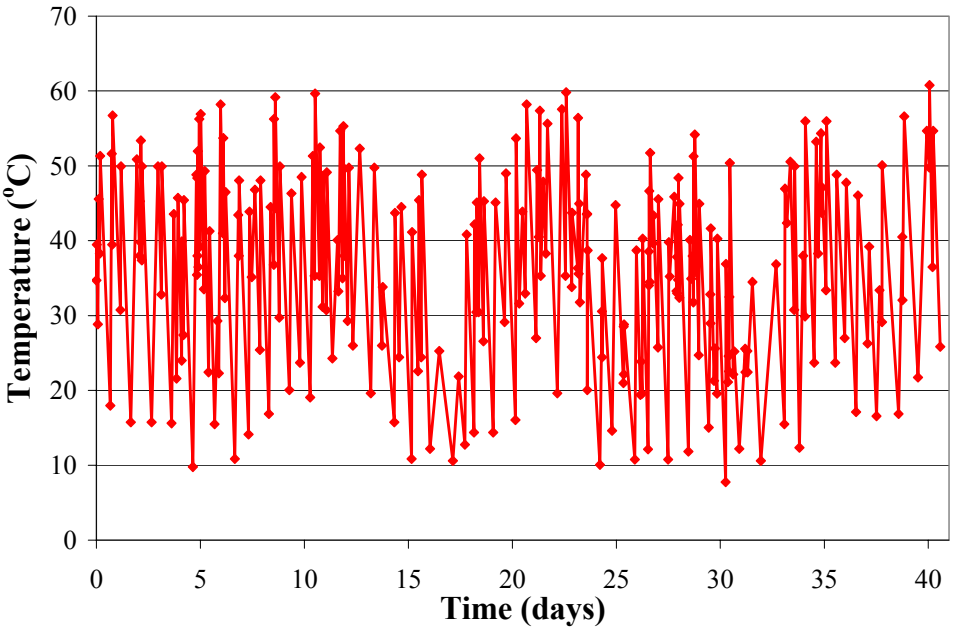

Figure 3.11: Monitored temperature converted to the peaks and valleys for case study-I

Figure 3.12 shows the power spectral density (PSD) vs. frequency for the out-of-plane vibration of the board. The PSD shown in the figure is the averaged value over the experiment duration. The frequency analysis range was 1 to 700 Hz. Accordingly the sampling rate and sample size were selected to be 1800 samples/second and 1024 samples.

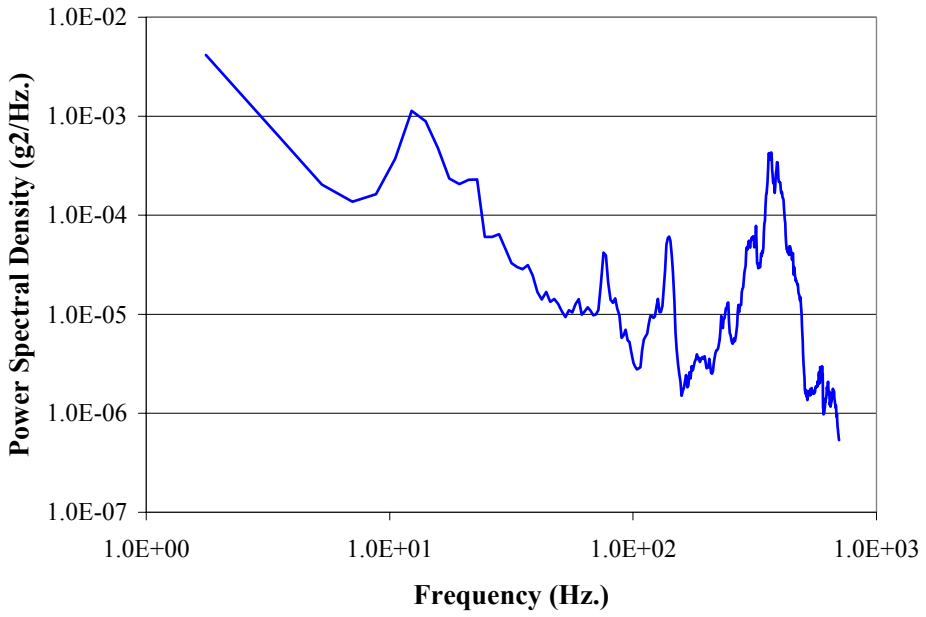

Figure 3.12: Power spectral density (PSD) vs. frequency plot for case study-I

The damage accumulation in the circuit card assembly was determined using calcePWA software. The output of the 3-parameter rainflow cycle counting algorithm and the power spectral density (PSD) vs. frequency data described above were used as input to the software. The displacements of the board and each component due to vibration were estimated through finite element analysis. Figure 3.13 shows the estimated displacement of the board. The reference point for the shown displacements was chosen to be the clamping points. The curvature along the horizontal axis of the board was found

to be constant (1.1 x 10^{-3} / inch), which indicated the equal amount of damage for all solder joints due to vibration.

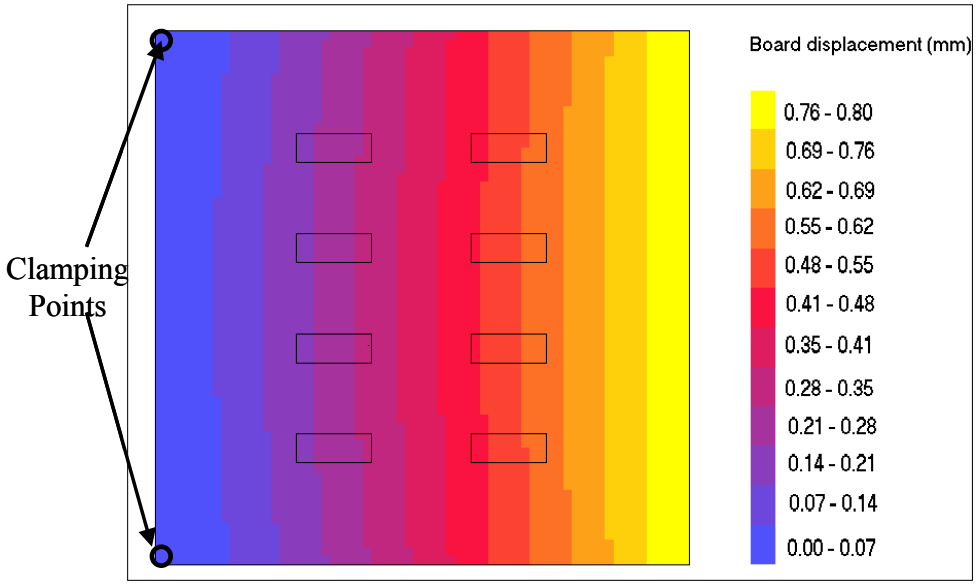

Figure 3.13: Estimated board displacement due to vibration for case study-I

An accident occurred during case study-I, where the car used for experiment was hit by another car. Vibration events with high g-values were recorded during the crash and during dis-engagement of the cars. The maximum g-levels for these events were an order of magnitude higher than normal conditions. Figure 3.14 shows the vibration event with highest g-level recorded during the crash. In this case the maximum value of acceleration was from +22g to –23 g (45 g peak-to-peak) as compared to 2g in case of normal random vibration. The highest g-level recorded during dis-engagement of the cars was + 9g to –9g (18 g peak-to-peak).

Under high levels of vibration, there is a chance of failure of the circuit card assembly if the stress under maximum acceleration exceeds the material strength of the solder joints. This failure due to shock is considered to be due to overstress mechanism.

Overstress models are usually used to find out whether the board can sustain the impact. An overstress analysis was conducted using calcePWA for the maximum acceleration value (45 g peak to peak), which showed no overstress failure.

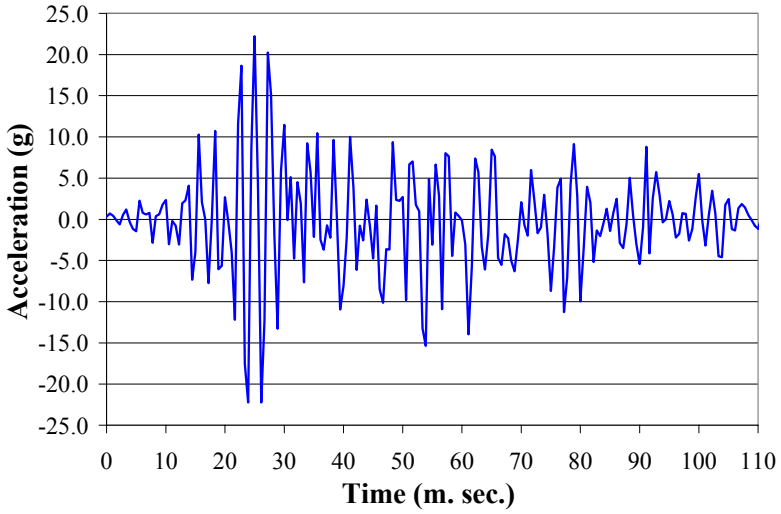

Figure 3.14: Recorded vibration event during the car accident. The maximum acceleration values were from +22 g to –23 g.

Hence a random vibration analysis was conducted with the PSD data obtained from all the events recorded during the crash and dis-engagement of the cars. The random vibration analysis resulted in maximum of 15% accumulated damage of the solder joints of the board. A more detailed section on the random vibration analysis is given in appendix-3.

Accumulated damage[9] was estimated using the physics-of-failure models and Palmgren-Miner theory on a daily basis. The results obtained are shown in the form of a bar chart (Figure 3.15).

[9] Estimated damage of 100% corresponds to the predicted end-of-life of the board.

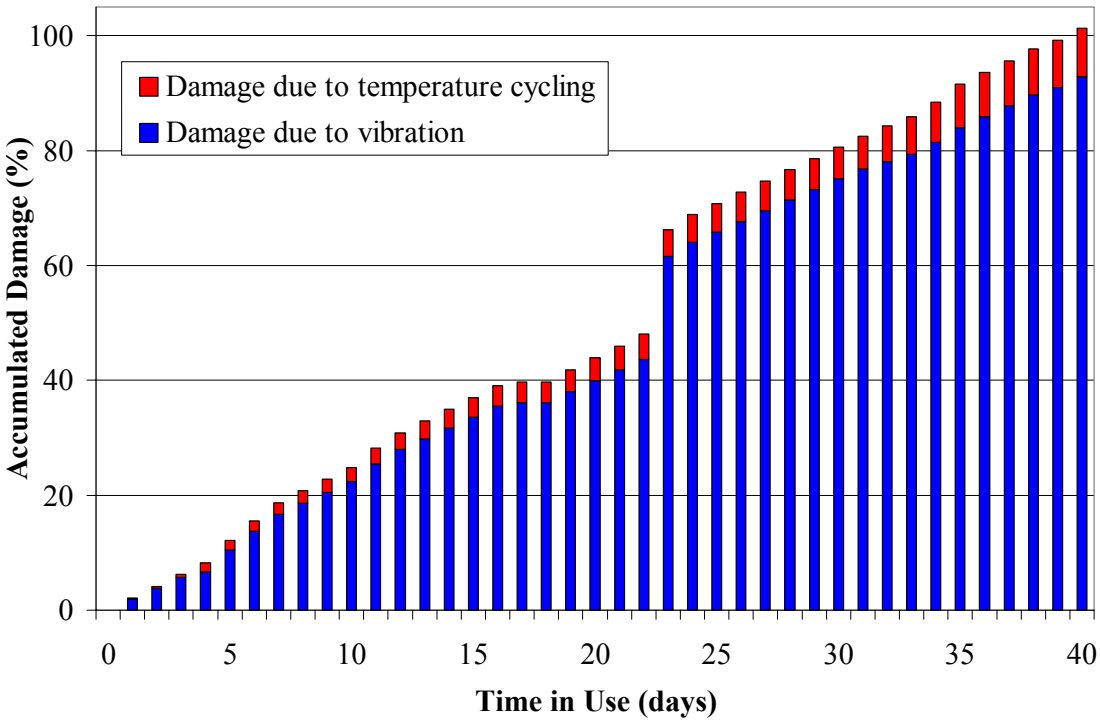

Figure 3.15: Accumulated damage estimated using calcePWA and Miner's rule for case study-I

Figure 3.16 shows the measured resistances of solder joints as a function of time. These resistance values were measured on a daily basis with the car engine off. The plot also shows the occurrences of the resistance spikes. The actual life of the circuit card assembly found to be 39 days according to the failure criteria.

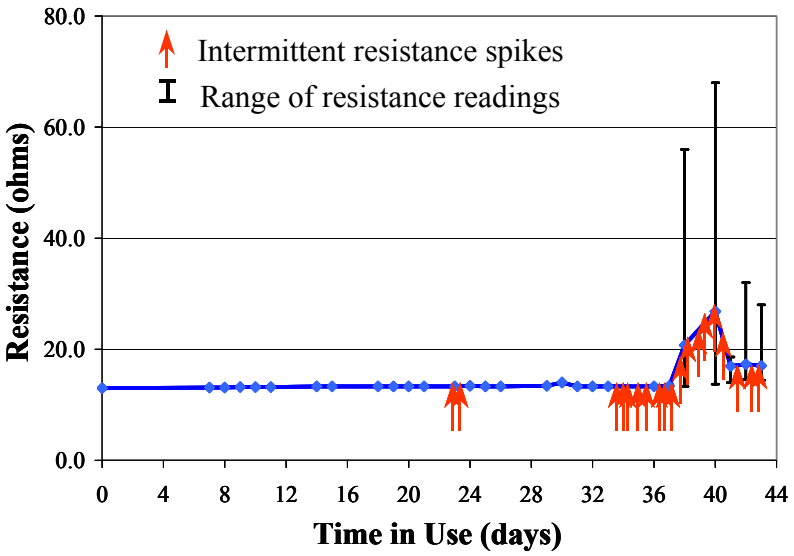

Figure 3.16: Resistances of the solder joints along with the intermittent resistance spikes for case study-I

Figure 3.25 shows the estimated remaining life and the actual life for the experiment. Initial predictions based on the similarity analysis and SAE environmental handbook data were 25 days and 34 days respectively. The estimated life based on life consumption monitoring with out taking into account the accident is 46 days. There was a drop in estimated life of the circuit card assembly by 6 days because of the accident. Hence the final estimated life is 40 days. The actual life based on resistance monitoring is 39 days, which is close to the estimated life based on life consumption monitoring.

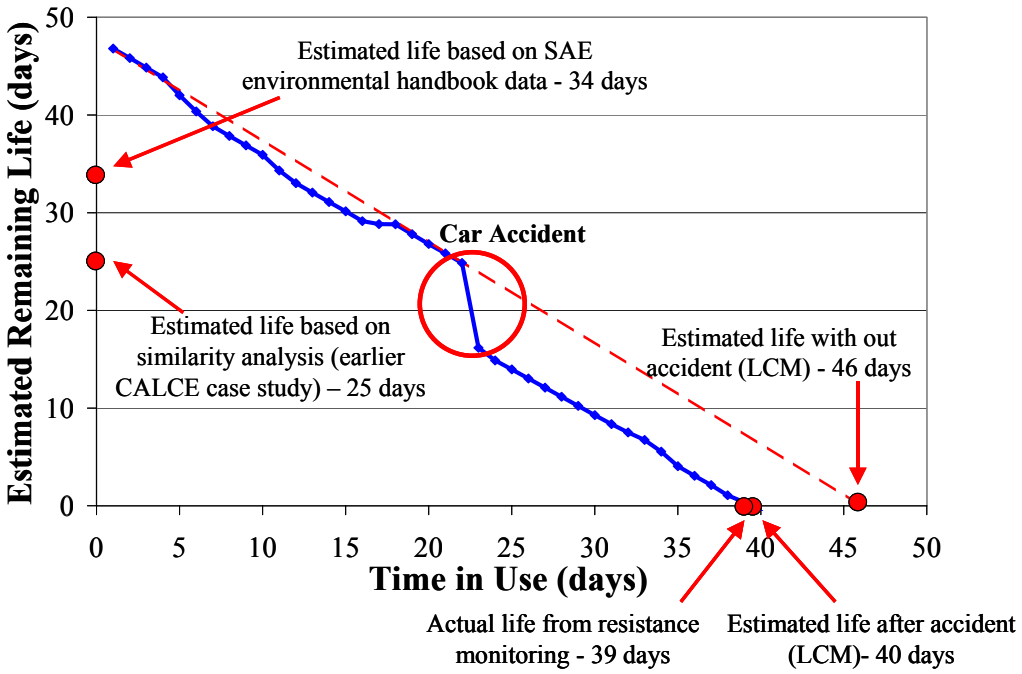

Figure 3.17: Remaining life estimation summary for case study-I

All solder joints of the test board assembly were photographed with the help of optical microscope from time to time during the experiment. Two of the solder joints showed cracks at a magnification of 50.

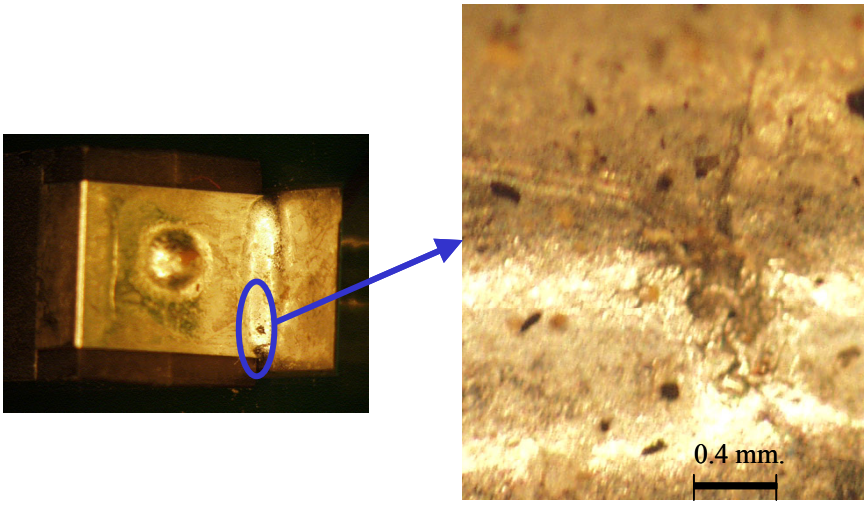

Figure 3.18: Crack in one of the solder joints

3.8.2 Case Study-II

A 2nd case study was conducted to demonstrate the life consumption monitoring methodology. There were some changes in the experimental setup in order to compare the in-plane and out-of-plane accelerations of the test board during the experiment.

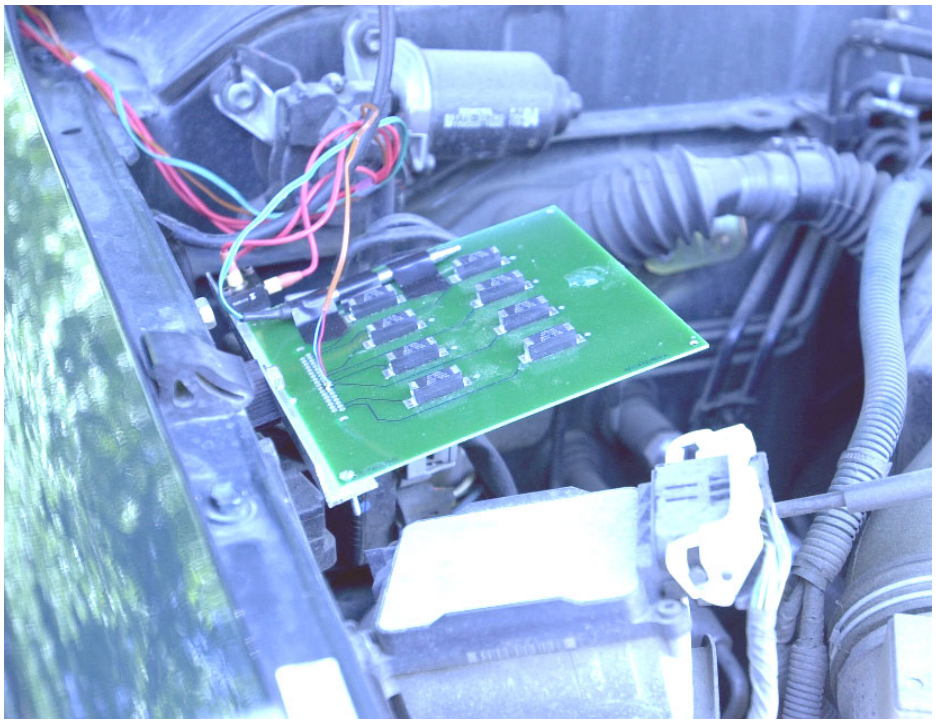

Figure 3.19: Experimental setup for case study-II

The temperature sensor used for the case study was the same as case study-I (Kele's Model STR-91S two-wire strap-on RTD sensor). A 3-D piezoelectric (Endevco's Model 2228C) accelerometer was mounted on one of the clamping points of the test board to measure accelerations in all 3 directions (out-of-plane acceleration for the board, acceleration along the car motion and the transverse direction). Figure 3.19 shows the experimental setup for case study- II.

Figure 3.20 shows the temperature variations on the test board for 66 days. Each data point is separated at an interval of one minute. The figure shows that the maximum temperature seen by the circuit card assembly is 89 ^{o}C, which is well below the glass transition temperature of FR-4 (130 ^{o}C) and the rated temperature of the inductors (125 ^{o}C). The minimum temperature seen by the circuit card assembly is 4 ^{o}C.

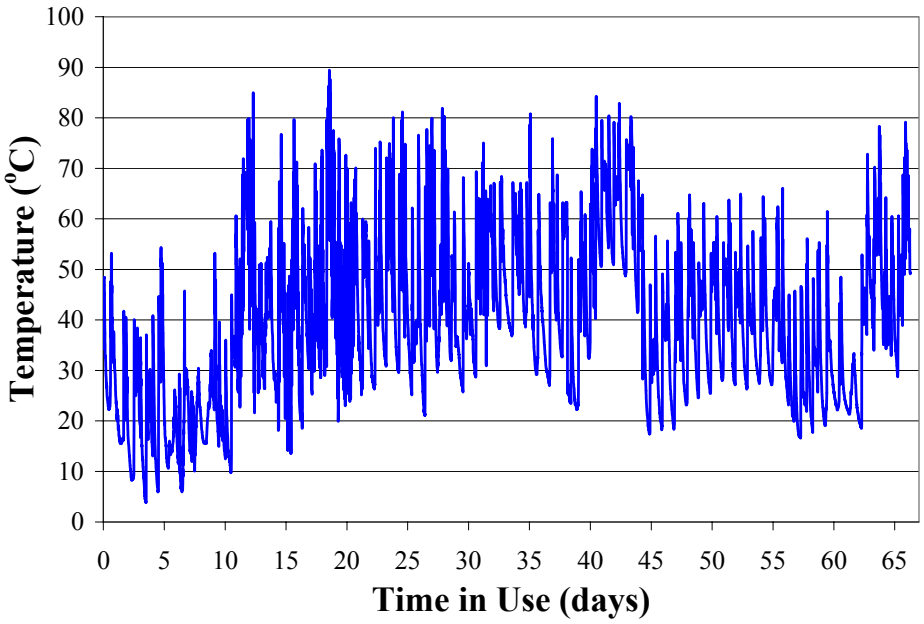

Figure 3.20: Monitored temperature for case study-II

The temperature vs. time history for 66 days was converted to an equivalent sequence of peaks and valleys using the ordered overall range (OOR) method. For this analysis the reversal elimination index was chosen to be 0% like case study-I. Figure 3.21 shows the acquired temperature data converted to peaks and valleys. The temperature-time history was converted to temperature cycles using the 3-parameter rainflow cycle counting method. 423 temperature cycles were identified for case study-II.

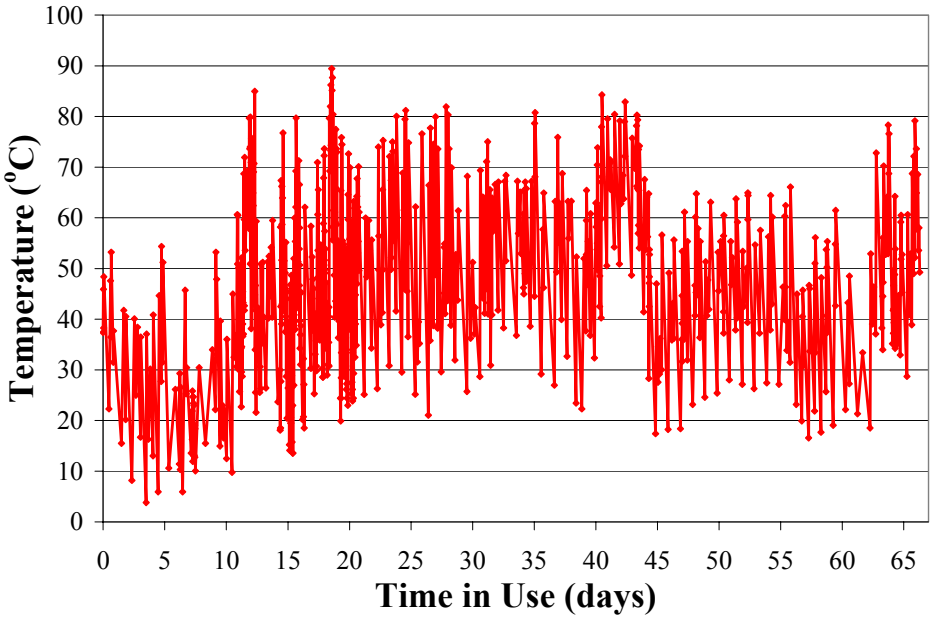

Figure 3.21: Monitored temperature profile converted to the peaks and valleys for case study-II

Figure 3.22 shows the power spectral density (PSD) vs. frequency plots for three different directions (out-of-plane acceleration for the board, acceleration along the car motion and the transverse direction) averaged over the experiment duration for frequency range of 1 to 700 Hz. The out-of-plane vibration was found to be at least 2 orders magnitude higher than the other directions. Further according to studies conducted by Steinberg, stress in the solder joints can be related to the out-of-plane displacement of the board [60]. Hence only out-of-plane (z-direction) vibration was used for vibration analysis.

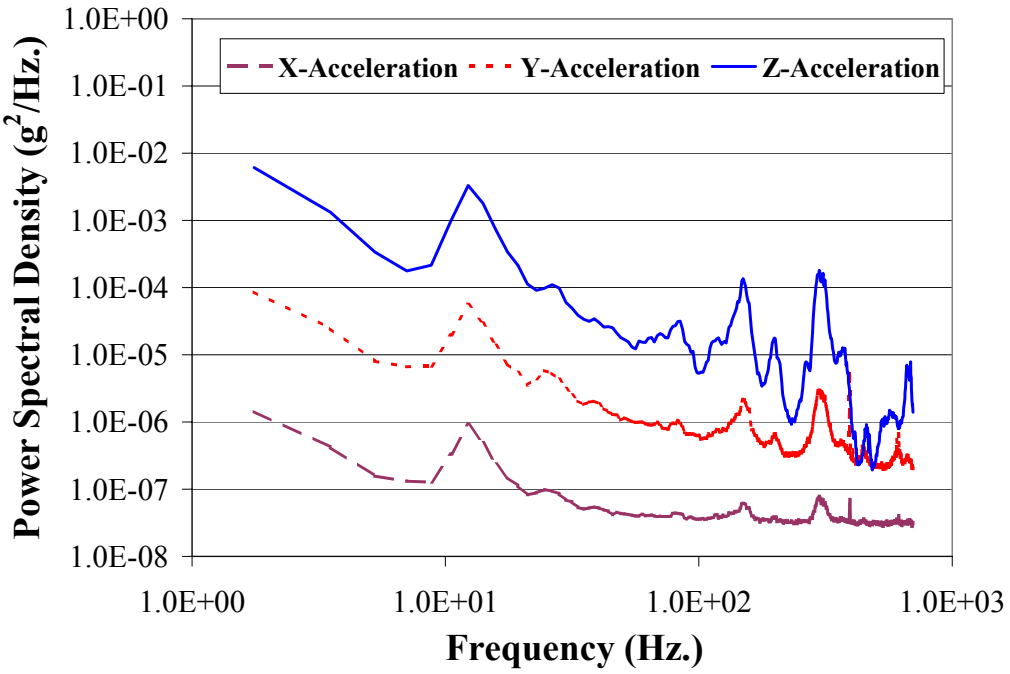

Figure 3.22: Power spectral density (PSD) vs. frequency plots for case study-II

The damage accumulation in the circuit card assembly was determined using calcePWA. The output of the 3-parameter rainflow cycle counting algorithm and the power spectral density (PSD) vs. frequency data were used estimate the damage. The displacements and radius of curvatures under each component were estimated through numerical analysis. The radius of curvature along the horizontal axis of the board is constant which predicts the same amount of damage accumulation in all solder joints as in case of case study-I. Figure 3.23 shows the results of the damage analysis in the form of a bar chart.

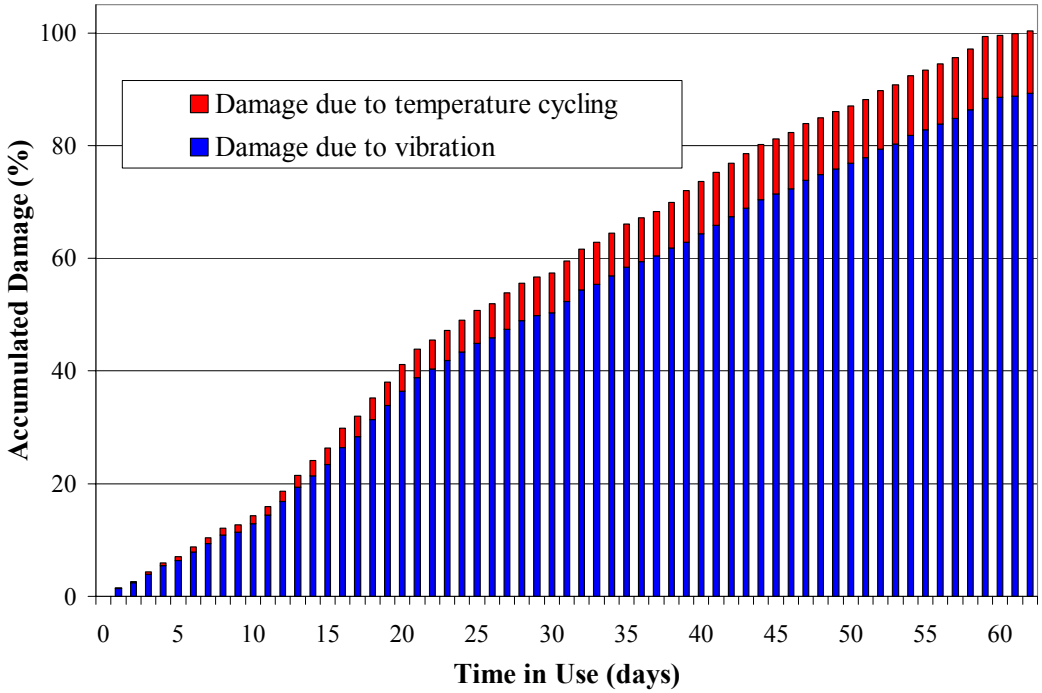

Figure 3.23: Accumulated damage for case study-II

Figure 3.24 shows the measured resistances of solder joints as a function of time with the corresponding ranges. These resistance values were measured on a daily basis. It can be seen from the plot that there is a gradual change in resistance through out the experiment starting from an average value of 12.8 ohms to a value of 14.6 ohms. The plot also shows the occurrences of the resistance spikes. The actual life of the circuit card assembly found to be 66 days according to the defined failure criteria, i.e., fifteen consecutive resistance spikes were observed on the 66th day.

Figure 3.25 shows the estimated remaining life and the actual life for the experiment. Initial predictions based on SAE environmental handbook data and the 1st case study were 33 days and 46 days respectively. The predicted remaining life based on

the life consumption monitoring methodology is 61 days, which is a conservative estimation of the failure (66 days).

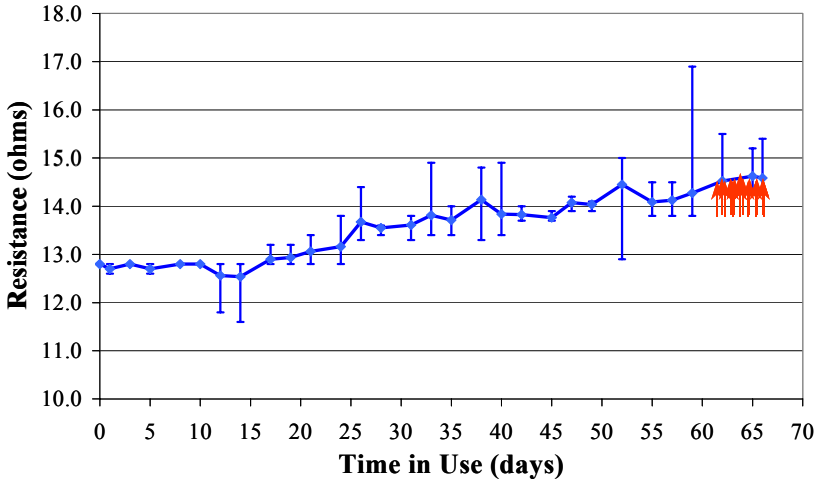

Figure 3.24: Resistances of the solder joints along with the intermittent resistance spikes for case study -II.

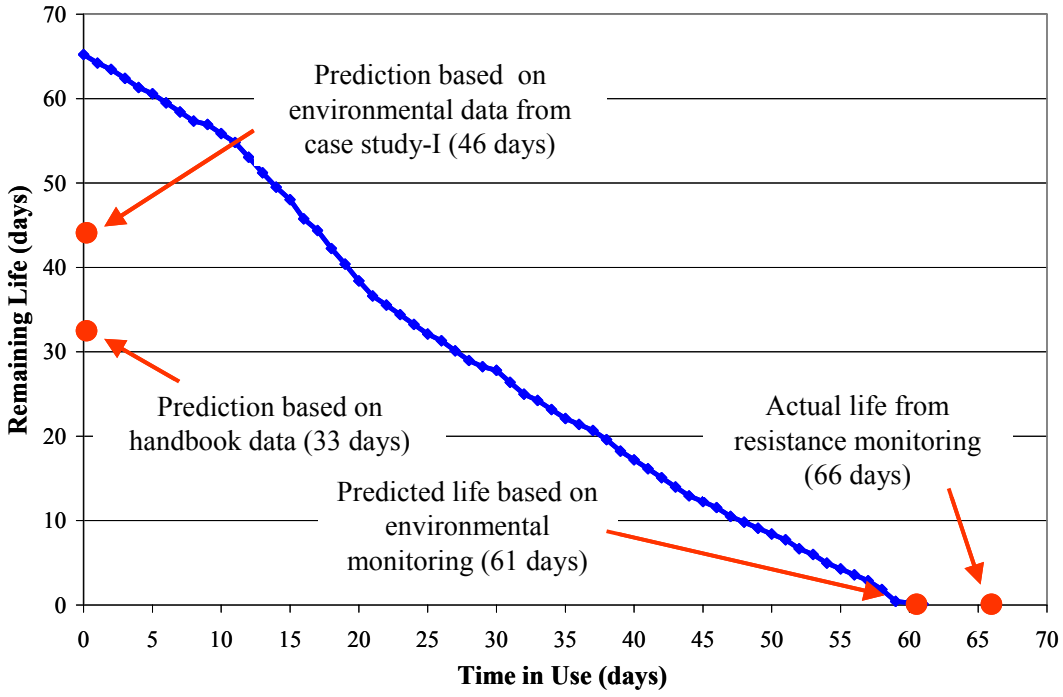

Figure 3.25: Remaining life estimation summary for case study-II

All solder joints of the test board assembly were photographed with the help of optical microscope at the end of the experiment as in case study-I. A visible crack was observed at the knee of a solder joint at a magnification of 50.

3.8.3 Comparison between case study-I and II

A comparison between the case study-I and case study-II is given in Table 3.4. Environmental temperature values are higher for case study-II compared to case study-I. This difference in temperature is because case study-I was conducted in winter and case study-II was conducted in summer. Power spectral density (PSD) values for case study-II are lower compared to case study-I. Difference in PSD values arises because of road conditions

Table 3.4: Comparison between case studies I and II

	Case Study I	**Case Study II**
Temperature	Avg. 30 ^{o}C Max. 61 ^{o}C	Avg. 41 ^{o}C Max. 89 ^{o}C
PSD value	8.73e-3 g^2/Hz. (max.)	6.09e-3 g^2/Hz. (max.)
Predicted life using life consumption monitoring	40 days	61 days
Actual life based on resistance monitoring	39 days	66 days
% Damage due to temperature	5 %	13%
% Damage due to vibration	95%	87%
Type of failure	Cracks in solder joints	Cracks in solder joints
Electrical indication of failure	• Intermittent resistance spikes • Permanent resistance increase of the solder joints (16 %)	• Intermittent resistance spikes • Permanent resistance increase of the solder joints (14 %)

4 SUMMARY AND DISCUSSION

This thesis describes a life consumption monitoring methodology for electronic products. Steps involved in the methodology have been explained in the thesis. Two example case studies were conducted to demonstrate the methodology for real life applications. The case studies were conducted in automobile underhood environment. Solder joint fatigue was identified as the dominant failure mechanism for the chosen environment based on failure modes, mechanisms, and effects analysis (FMMEA) and virtual reliability assessment. Accordingly, the following steps in the life consumption monitoring were customized. Ordered overall range algorithm and 3-parameter rainflow cycle counting algorithms were combined to develop a suitable data simplification scheme for the chosen conditions. Proper stress and damage models were identified and used along with the data simplification scheme for the case study conditions. An algorithm was developed to estimate the remaining life of the electronics for the case studies based on the results from stress and damage models. The steps followed for case studies can be summarized as follows:

- Two identical test board assemblies were mounted in a cantilever fashion under-the-hood of an automobile.
- Failure modes, mechanisms, and effects analysis (FMMEA) was conducted along with virtual reliability assessment to determine the dominant failure mechanism for the given life cycle environment. Solder joint fatigue was identified as the dominant failure mechanism for the given environment.

- Temperature and vibration were identified as the environmental parameters for monitoring were identified based on inputs to the solder joint stress and damage models.
- Vibration and temperature data were monitored and simplified for compatibility with stress and damage models.
- Stress and damage models were used along with the remaining life estimation algorithm to determine the remaining life of the circuit card assemblies.
- Electrical performances of the circuit card assemblies were checked through resistance monitoring to determine their actual life.
- The predicted life of the test board assemblies were found to be in agreement with the experimental life.
- Remaining life of the test board assemblies were predicted with information from various sources. All estimation results were compared.

The remaining life values for the case studies mentioned in the paper were found to be very close to the experimental values, which can be explained by the following reasons. The circuit card assemblies were designed intentionally with large surface mount leadless inductors to precipitate failure solder joint fatigue much before other failure modes. Further the stress and damage models used for analysis using calcePWA are well calibrated for leadless components on a FR-4 printed circuit board. However, in more complex circuit card assemblies, the life estimation results are dependent on various other failure sites and mechanisms, which might result in higher amounts of error in the estimation.

4.1 Using Handbooks and Similarity Analysis to Determine Environmental and Operational Life Cycle Conditions

Life consumption monitoring process requires information on product geometry, material properties along with actual environmental and operational parameters in its life cycle environment. Once the product design is complete, its geometry and material properties can be obtained from various sources including design layout, manufacturer data sheets. However, until the beginning of product parameter monitoring, no information on environmental and operational parameters is available. For life estimation at this stage, life cycle information is taken either from environmental handbooks or data monitored in similar applications. Environmental handbooks are good sources of information for newly designed products. An example is data from SAE environmental handbook for automobile electronics. For the case studies mentioned in the paper, data from SAE environmental handbook resulted in 34 days of total life as compared to 66 days from the experiment in case study-II. This difference in the results can be because the SAE environmental handbook provides a generic set of data not pertaining to a specific car manufacturer or geographical location. Further the data available in SAE environmental handbook represents twenty year old information [43].

Another source of information is the data collected from sensors for same or similar products in a similar environment. This is possible only if the same product or a similar product is already in production and monitored data from sensors are available. This is called “using similarity to determine environmental and operational conditions”. A virtual reliability assessment based on case study-I gives a total life of 46 days, which

is different from a total life of 66 days in case of case study-II. This difference can be because of higher levels of vibration along with the car accident.

The process of using environmental data from handbooks or similarity analysis with stress and damage models is often very useful because it can provide a quick estimate of product life before spending a lot of time and money in environmental monitoring. However, as shown in the case studies, the results may not be very accurate as the process takes into account an approximate life cycle environment and does not account for any change in life cycle conditions. Sometimes a sudden change in product life cycle environment (e.g., accident of the automobile mentioned in case study-II) can have a catastrophic impact on its life.

In general, the actual life cycle environment that a product encounters is different from the statistically averaged values from handbooks. For automobile electronics, life cycle environment depends on road conditions (for vibration), geographical location and part of the year (for temperature, humidity). Hence after placing the product in the field conditions and obtaining information about the life cycle environment more precise information about remaining life can be obtained using the life consumption monitoring approach. If there is any change in the life cycle environment (e.g., the car accident mentioned in one of the case studies), there is an abrupt change in remaining life. By knowing the remaining life of the product after an accident, the product mission can be rescheduled to get intended life. This concept is known as “extension of life”, which explains how life consumption monitoring results can be used in real life.

Figure 4.1 shows the idealized remaining life vs. time plot for an electronic product. The time corresponding to 0% remaining life of the product gives the time-to-

failure of the product at a given load condition. This illustrates change of mission profile to achieve extension of life.

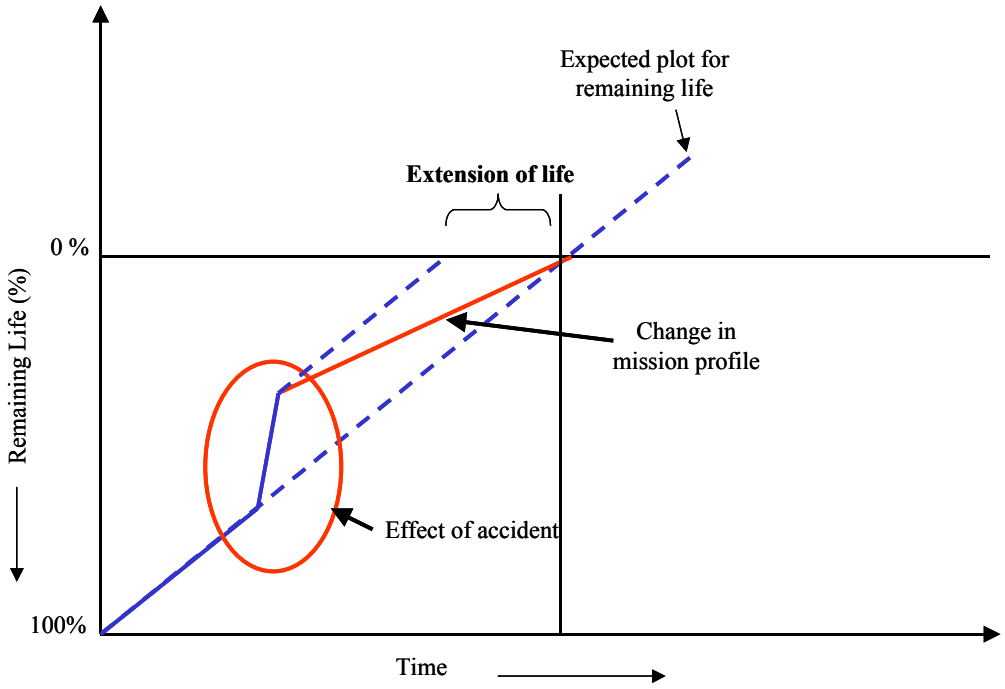

Figure 4.1: Extension of life based on life consumption monitoring results

4.2 Determining the Number of Data Points Required for Life Estimation

Total useful life of a product at any point on the remaining life vs. time plot can be estimated by adding the time in use (or x-coordinate) and the remaining life (or y-coordinate) at that point. However, this analysis is a one-point estimation and does not take into account the product usage trend. The product usage trend can be taken in account by extrapolating a trend line using the available remaining life data points. The intersection of the trend line with the time axis gives the total useful life of the product (see Figure 4.2).

The number of data points that can be considered for the trend line varies from two data points to all data points. “Cumulative past analysis for life estimation” is the life estimation process where all the available data points in the remaining life plot are used. On the other hand, “near past analysis for life estimation” is the life estimation process where only some of the data points are used. Results obtained can be different by using cumulative past and near past data if there is a large variation in the results from the damage models. This variation can occur from variation in environmental and operational parameters that are inputs to the damage models. An example of such variation is the result due to the car accident mentioned in one of the case studies.

Figure 4.2 explains the concept of cumulative past and near past analysis with the help of 24 data points from Figure 3.17 including the car accident. The plot shows that life estimation results (at the end of 24^{th} day) based on near past (i.e., three data points) and cumulative past (i.e., all data points). The near past analysis results differ from the cumulative past analysis and the actual results by 26%. This error reduces by using more number of data points for near past analysis. This explains the requirements to compare variations in results obtained using different number of data points.

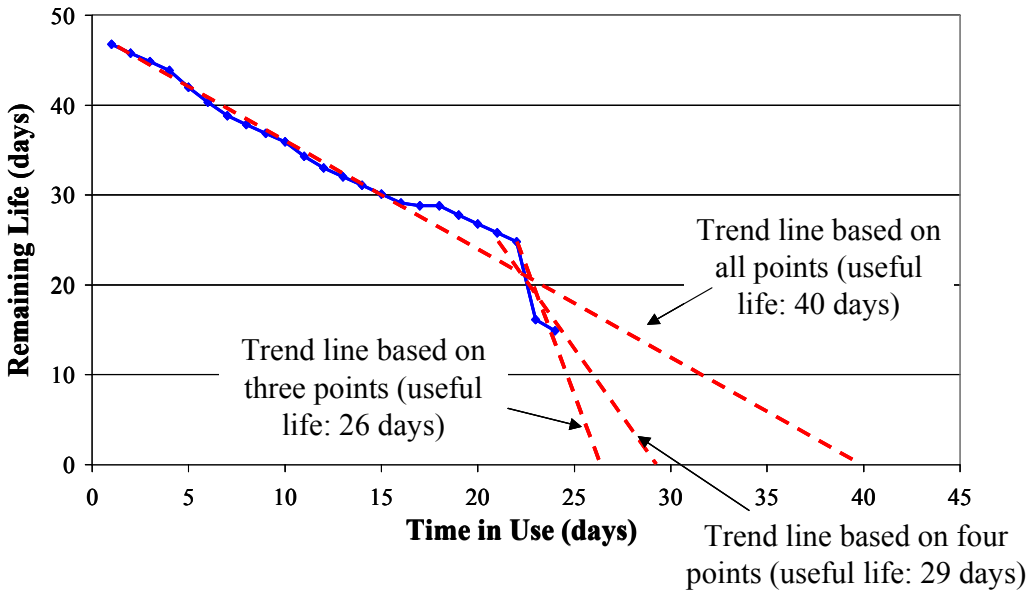

Figure 4.2: Cumulative past vs. near past for life estimation

As a rule of thumb, if the result using "n" data points ("n" starts from 2) and "n+1" data points differ by less than the acceptable remaining life (see section 2.7), "n" data points can be used for the analysis. More data points need to be considered if the variation is more than the acceptable remaining life. This concept takes into if the changes in damage model results (e.g., due to change in geographical location of the product or use in a different application) are expected to continue in future.

5 CONTRIBUTIONS

This thesis describes the development of a life consumption monitoring methodology for remaining life estimation of electronic products. The life consumption monitoring methodology has been described in a general way so that it can be extended to various electronics products. Failure modes, mechanisms, and effects analysis (FMMEA) and virtual reliability assessment are included in the methodology to identify the dominant failure mechanisms in a given life cycle environment. A process has been explained to identify the environmental and operational parameters based on the failure models for the dominant failure mechanism. An iterative method was described to estimate the remaining life based on the accumulated damage information obtained from stress and damage accumulation analysis.

Two case studies were conducted to demonstrate the life consumption monitoring methodology in automotive underhood applications. Monitored environmental data was used on a daily basis to estimate remaining life of two circuit card assemblies. The electrical performances of the circuit card assemblies were monitored throughout the experiments to determine field failure. The estimated life results were found to be in agreement with the actual life results.

Appendix I: Damage assessment model for temperature induced fatigue analysis

Failure of solder interconnects due to temperature cycling is a common problem in electronic hardware. Solder joint failures typically arise from fatigue due to thermal expansion mismatch

- Between the package and the board (global mismatch)
- Between interconnect, solder, board (local mismatch)

A common model for solder joint fatigue due to thermal fatigue is based on the work of Werner Engelmaier. The model uses a strain range as the metric for calculating cycles to failure. The calculation of strain range considers both global mismatch and the local mismatch in thermal expansion.

Assumptions associated with the model are:

- Fatigue failure of solder joints can be described as a power law similar to the Coffin-Mansion low cycle fatigue equation.
- Strain in the solder arises from global as well as local thermal expansion mismatch and the strain arising from local mismatch may be added to strain produced by global strain to get the global strain (worst case).
- In-plane deformations are large compared to out-of-plane warping.
- Complete stress relaxation occurs during the thermal cycle.

The Engelmaier's thermal fatigue model can be written in equation form as [45]:

$$N_f = \frac{1}{2}\left(\frac{\Delta\gamma_p}{2\varepsilon_f}\right)^{\frac{1}{c}}$$

where N_f is the mean number of cycles to failure, γ_p is the inelastic strain range and ε_f is a material constant (0.325 for eutectic solder).

The exponent c is known as the fatigue ductility coefficient and given by the following relation

$$c = -0.422 - \left(6 \times 10^{-4}\right) T_m + \left(1.74 \times 10^{-2}\right) \ln\left(1 + \frac{360}{t_d}\right)$$

where T_m is mean cyclic temperature of the solder in ^oC and t_d is the dwell time in minutes at the maximum temperature

The inelastic strain range $\Delta\gamma_p$ for the fatigue relationship is calculated by considering the response of the package assembly to the change in temperature. The stress state (stress and strain) is a function of the package, interconnect, and board geometry and material.

$$\Delta\gamma_t = \left|\Delta\gamma_g\right| + \left|\Delta\gamma_l\right|$$

The strain range due to global mismatch for leadless interconnects with eutectic can be approximated to be [45], [59].

$$\Delta\gamma_g = \frac{0.5FI}{h}\left(\Delta\alpha L T_b - \Delta\alpha L T_c\right)$$

where F is the user defined calibration factor [10]I is the calibration factor [11], h = height of solder joint (mils) and T_c, T_S = temperatures of component and printed circuit board (^oC).

[10] This empirical correction factor accounts for idealized assumptions (F varies from 0.5 to 1.5, typical values are around 1.0 and are determined by fitting fatigue life results to predicted life)

[11] This factor is calibrated in calcePWA software based on various experimental results

$$\Delta\alpha LT_c = \sqrt{\left(\left(L_x\alpha_{cx}\right)^2 + \left(L_y\alpha_{cx}\right)^2\right)}\left(T_c^{\max} - T_c^{\min}\right)$$

$$\Delta\alpha LT_b = \sqrt{\left(\left(L_x\alpha_{bx}\right)^2 + \left(L_y\alpha_{by}\right)^2\right)}\left(T_b^{\max} - T_b^{\min}\right)$$

where α_{cx}, α_{cy}, α_{bx} and α_{by} are the coefficients of linear thermal expansion for component and board, in x and y directions respectively (ppm/^{o}C); L_x and L_y are the span of interconnect in x and y directions (inch).The strain range due to local thermal expansion mismatch can be approximated to be

$$\Delta\gamma_l = \frac{\Delta T\Delta\alpha \sinh\left(Al_{eff}\right)}{bA\cosh\left(Al_{eff}\right)}$$

where G is the shear modulus of the solder, b is the solder thickness, E_l is the modulus of elasticity of lead, E_b is the modulus of elasticity of the board, t_l is the lead thickness, and t_b is the board thickness. The factor A is given by

$$A = \sqrt{\frac{G}{b}}\sqrt{\left(\frac{1}{E_l t_l} + \frac{1}{E_b t_b}\right)}$$

For leadless packages, $l_{eff} = 0$ and hence $\Delta\gamma_l = 0$.

Appendix II: Damage assessment model for vibration induced fatigue analysis

For harmonic vibrations, maximum acceleration of the printed circuit board (PCB) can be written in terms of maximum displacement, Z_o as

$$a_{\max} = \omega^2 Z_o$$

In terms of g's

$$G_{\max} = \frac{a_{\max}}{g} = \frac{\omega^2 Z_o}{g} = \frac{(2\pi f)^2 Z_o}{g}$$

The maximum displacement can be written in terms of natural frequency, f_n as

$$Z_o = \frac{9.8\, G_{in}\, Q}{f_n^{\,2}}$$

where G_{in} is the input acceleration to the PCB and Q is the transmissibility of the PCB at its natural frequency. For natural frequencies between 200-400 Hz., a good approximation is $Q = \sqrt{f_n}$ [60].

Failures due to high cycle fatigue (vibration induced) in solder joints can be described by the following relationship:

$$\sigma N_f^{\,b} = Constant$$

where σ is the solder joint maximum stress amplitude, N_f is the cycles to failure and b is a material property. Steinberg assumes that the stress in the solder joints can be directly related to the out of plane displacement of the board, i.e.,

$$Z N_f^{\,b} = Constant$$

Hence, $Z_1 N_1^{\,b} = Z_2 N_2^{\,b}$

Solving for N_2,

$$N_2 = N_1\left(\frac{Z_1}{Z_2}\right)^{\frac{1}{b}}$$

where N_1 and Z_1 are the life and displacement from Steinberg's equation, N_1= 10,000,000 for sinusoidal and 20,000,000 cycles for random vibration [60], and Z_2 is the maximum board displacement amplitude as given by equation 9. Through extensive testing and design experience of PCB assemblies, Steinberg developed an empirical equation for maximum allowable displacement, Z_1

$$Z_1 = \frac{0.00022B}{ct\sqrt{L}}$$

The life of the components also depends on where they are placed. This variation in life is a function of radius of curvature under the components and can be included in the relationship as:

$$N_2 = N_1\left(\frac{Z_1}{Z_2\ \sin(\pi x)\sin(\pi y)}\right)^{\frac{1}{b}}$$

where x, and y are the non-dimensional board co-ordinates of the component center.

Random vibration response is usually discussed in terms of the root mean square (RMS) acceleration. When the distribution is normal, the RMS value is the mean of the distribution. To account for the 3σ extremes for random vibration [60]

$$Z_o = 3\ \left[\frac{9.8\ G_{rms}}{f_n{}^2}\right]$$

RMS acceleration of the board is approximated as

$$G_{rms} = \sqrt{\frac{\pi}{2} PSD\ f_n\ Q}$$

For the case study, the board displacement under each solder joint is estimated by finite element method using the calcePWA software.

In shock environment, Steinberg [60] uses a simple rule of thumb that in shock environment of less than few thousand total cycles, the maximum allowable displacement of the PWB is:

$$d = \frac{0.00132B}{ct\sqrt{L}}$$

where B is the length of the PWB edge parallel to the component, L is the length of the components (inches), c is a constant depending on the package type.

Appendix III: Analysis of Car Accident for Case Study-I

The car accident mentioned in one of the case studies, resulted in high levels of vibration during and after the accident. The data recording device recorded a number of high vibration events. The maximum g-levels for these events were an order of magnitude higher than normal conditions. The event with highest acceleration was selected for input to calcePWA shock analysis module.

Shock analysis is typically conducted with the help of an overstress model. Overstress failure of solder joints is defined as failure due to stresses that exceed the ultimate strength of the solder. Shock analysis of solder joints can be conducted with calcePWA software for an individual shock pulse. A shock pulse can be specified in calcePWA by the type of pulse (e.g., half sine, unit impulse, terminal sawtooth), maximum acceleration value and its time duration. The shock analysis can only determine whether there is an overstress failure.

The identified event was found to contain a number of acceleration peaks. The maximum peak-to-peak acceleration (45 g) was modeled in calcePWA as a half sine pulse for shock analysis. The time duration of the 45 g pulse was determined as 3 milliseconds from the recorded data. calcePWA shock analysis showed no overstress failure. Since the analysis was conducted at the worst case conditions, it was concluded that no overstress failure occurred during the car accident. The electrical resistances of the solder joints also confirmed no failure. No information on the accumulated damage could be obtained from the shock analysis. However, this does not mean that there is no accumulated damage in the circuit card assembly because of the accident.

Since shock analysis was conducted for a duration of 3 milliseconds with a single pulse, the possibility of accumulated damage could not be ruled out. Further, high vibration levels lasted for half an hour[12], which confirmed the fact that there can be accumulated damage. Hence an attempt was made to analyze the car accident using the existing random vibration models.

Random vibration damage analysis is typically conducted using high cycle fatigue models, which require specification of more than 10^4 cycles. The fundamental frequency of the circuit card assembly for the given mounting system was estimated to be 25.7 Hz from calcePWA. It was found that thirteen vibration cycles were possible per event (time duration of approximately 500 milliseconds) at this fundamental frequency. This precluded the possibility of random vibration analysis of individual events. To overcome this limitation, all events recorded over a duration of 30 minutes were used to estimate the power spectral density (PSD). The estimated PSD vs. frequency is shown in Figure. 1. A random vibration analysis was conducted using calcePWA with this PSD information for a time duration of 30 minutes. Table. 1 gives the power spectral density vs. frequency input to calcePWA. Random vibration analysis of the shock showed maximum 15% damage on the solder joints and reduction of life by 6 days. Analysis of the car accident was possible because of the availability of all the data points over the interval of time.

[12] High vibration events were observed from the moment of the car accident to the moment when the circuit card assembly and the sensors were removed to repair the car. The time frame also included the vibration event during disengagement of the cars.

Table. 1: Power spectral density vs. frequency input to calcePWA

Frequency (Hz.)	1.76	12.3	17.6	26.4	76	141	248	378	527	693
Power Spectral Density (g^2/Hz.)	0.225	0.39	0.632	0.029	0.034	0.645	0.52	0.024	0.007	0.15

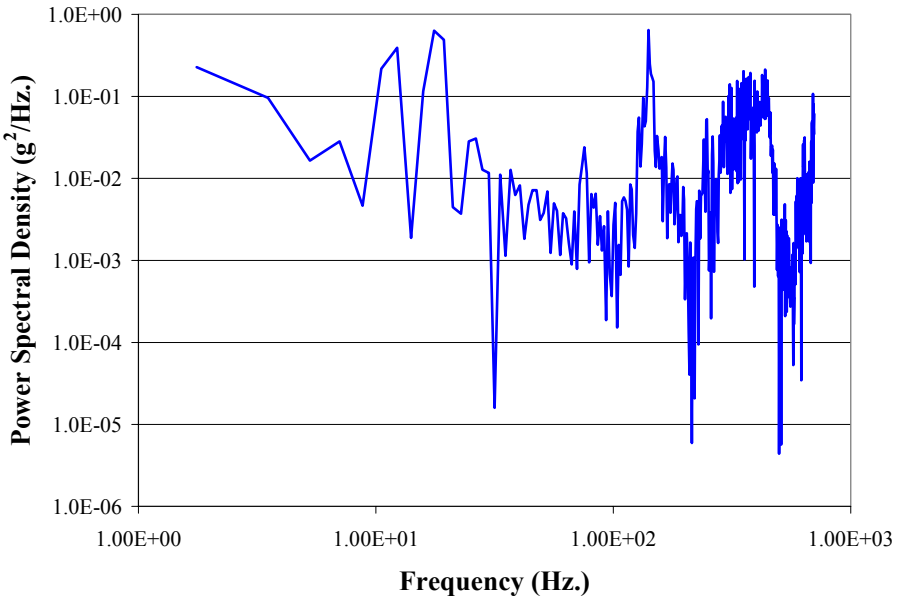

Figure. 1: Power spectral density (PSD) vs. frequency for the car accident

Appendix IV: Effect of temperature data reduction on prediction accuracy of life consumption monitoring

To estimate the effect of temperature data reduction on the prediction accuracy of life consumption monitoring, the temperature data collected from case study-II was analyzed. For this analysis, the data was sampled at the rate of one data point per ten minutes. The collected temperature data was simplified using the ordered overall range (OOR) method and the 3-parameter rainflow cycle counting algorithm. A program was developed to combine the OOR method, 3-parameter rainflow cycle counting algorithms and Engelmaier's model for solder joint fatigue to estimate the accumulated damage. The accumulated damage of an individual solder joint was simulated with different values of reversal elimination indices, 's' (from 0 to 90%). The geometry and the properties of the inductors and solder joints were used for the analysis.

For each value of reversal elimination indices, error was estimated. The error values are compared to a situation where all reversals are preserved (i.e., reversal elimination index, $S = 0.0$). Figure. 2 shows a plot of error % as a function of reversal elimination index.

$$\text{Error } \% = \left| 1 - \frac{\text{Damage Accumulation}}{\text{Damage Accumulation (S = 0.0)}} \right| * 100$$

It can be seen from Figure. 2, the value of error is very low for a reversal elimination index (s) values up to 0.2 (i.e., a peak valley sequence is selected only if their difference is greater than 0.2 * difference between the highest peak and the lowest valley). For 's' values greater than 0.2, the error value increases rapidly causing almost 85% error at s=0.9.

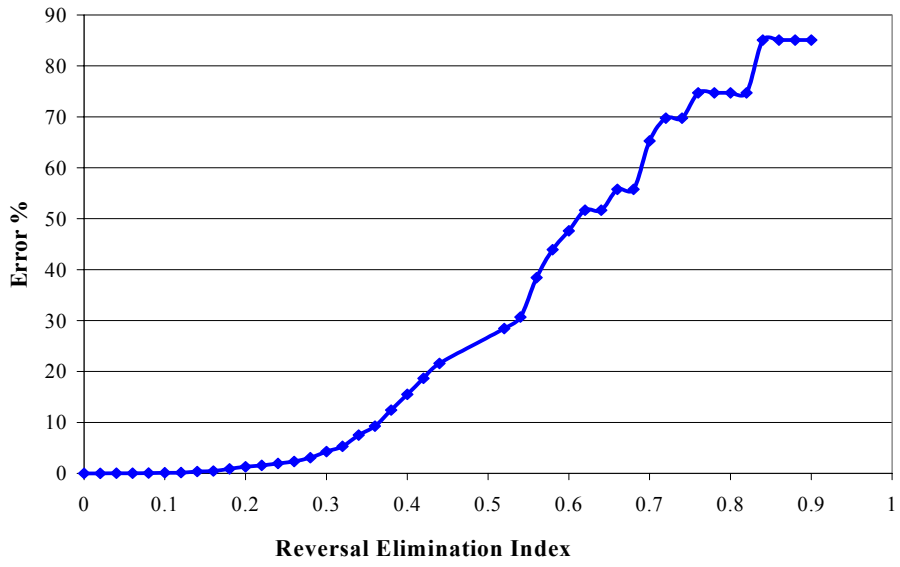

Figure. 2: Estimated error as a function of reversal elimination index

The number of remaining data points (reversals) in the load history decreases with increase in '*S*'. This is because the cut off value (i.e., '*S*' times the difference between highest peak and the lowest valley) increases with increase in '*S*' given the same load history (see Figure 3.5). The fraction of data reduction is defined as:

$$\text{Fraction Data Reduction} = \frac{\text{No. of Remaining Data Points}}{\text{Total no. o f Data Points}}$$

Figure. 3 shows the plot of error % as a function of fraction data reduction. It can be seen that less than 5% error is caused by 96 % data reduction in this case. In other words, only 5 % of the data points constitute the most damaging reversals for thermal fatigue analysis in case of solder joints in electronics. Hence the data reduction method developed can be effectively used for eliminating less damaging reversals.

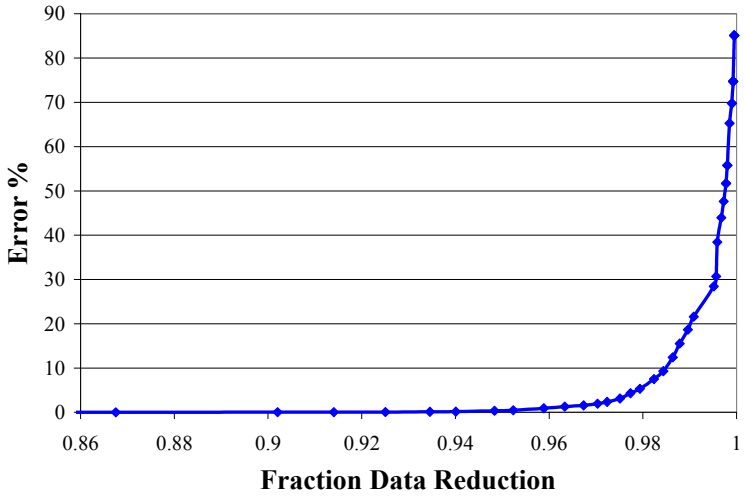

Figure. 3: Estimated error as a function of data reduction

Different sampling rates result in different number of data points for a given interval of time. However, a lot of data points are not useful for the temperature analysis as the OOR algorithm takes into account only those data points that are either peaks or valleys. Hence the number of data points that are neither peaks nor valleys increase with sampling rate. As a result, even with reversal elimination index of 0.0 (i.e., all peaks and valleys are counted), there is high amount of data reduction in case of higher sampling rate. As long as the sampling rate is above certain limit where all the peaks and valleys can be recorded, the maximum number of useful data points is independent of sampling rate (i.e., all peaks and valleys). Specification of a reversal elimination index in such a case will result in equal number of data points remaining after the OOR analysis. This will result in equal amounts of damage and hence equal amounts of error for all sampling rates. In other words, estimated error is independent of reversal elimination index beyond a certain sampling rate. However, the data reduction will be more for higher sampling rate for a given amount of error because of higher data reduction at reversal elimination index of 0.0.

REFERENCES

[1] IEEE Reliability Society, " IEEE Std 1413" IEEE Standard Methodology for Reliability Prediction and Assessment for Electronic Systems and Equipment," New York, NY, January 1999.

[2] Ramakrishnan, A., Syrus, T., and M. Pecht, "Electronic Hardware Reliability," *The Modern Microwave and RF Handbook*, pp. 3-102 to 3-121, CRC Press, Boca Raton, FL, 2000.

[3] Pecht, M., Product Reliability, Maintainability, and Supportability Handbook, CRC Press, New York, NY, 1995.

[4] Beder, S., "Making Engineering Design Sustainable," *Transactions of Multi-Disciplinary Engineering Australia*, Vol. GE17, No. 1, pp. 31-35, June 1993.

[5] Kelkar, N., Dasgupta, D., Pecht, M., Knowles, I., Hawley, M. and D. Jennings, "Smart Electronic Systems for Condition-Based Health Management," *Quality and Reliability Engineering International*, Vol. 13, pp. 3-7, 1997.

[6] Rao, B.K.N., Handbook of Condition Monitoring, Elsevier Science Publishers Ltd., Oxford 1996.

[7] Mobley, R.K., An Introduction to Preventive Maintenance, Van Nostrand Reinhold, New York, NY 1990.

[8] NIST, "Condition-based Maintenance," Advanced Technology Program Position Paper, http://www.atp.nist.gov/files/cbm_wp1.pdf (08/01/2003)

[9] Borinski, J.W., Meller, S.A., Pulliam, W.J., Murphy, K.A.,and J. Schetz, "Aircraft health monitoring using optical fiber sensors," *Proceedings of the 19th Digital Avionics Systems Conference*, Vol. 2, pp. 6D1/1 –6D1/8, 2000.

[10] Cooper, K.R., Elster, J., Jones, M., and R. G. Kelly, "Optical fiber-based corrosion sensor systems for health monitoring of aging aircraft," *AUTOTESTCON Proceedings, IEEE Systems Readiness Technology Conference*, pp. 847-856, 2001.

[11] Borinski, J.W., Boyd, C.D., Dietz, J.A., Duke, J.C., and M. R. Home, "Fiber optic sensors for predictive health monitoring," *AUTOTESTCON Proceedings, IEEE Systems Readiness Technology Conference*, pp. 250-262, 2001.

[12] Goldfine, N., Schlicker, D., Sheiretov, Y., Wailiabaugh, A., Zilberstein, V., and D. Grundy, "Surface mounted and scanning periodic field eddy-current sensors for structural health monitoring," *IEEE Aerospace Conference Proceedings*, Vol. 6, pp. 3141-3152, 2002.

[13] Kent, R.M**,** "Fiber ultrasonics for health monitoring of composites," *Proceedings of the 19th Digital Avionics Systems Conference*, Vol.2, pp. 6D3/1 -6D3/6, 2000.

[14] Larson, E.C., and B. E. Parker Jr., "A subspace-based approach to structural health monitoring," *Proceedings of 19th Digital Avionics Systems Conference*, Vol.2, pp. 6C5/1 -6C5/8, 2000.

[15] Yen, G. and Tuang Bui "Health monitoring of vibration signatures in rotorcraft wings," *Proceedings of IEEE Aerospace Conference,* Vol.1, pp. 279 –288, Feb 1997.

[16] Yen, G., "Health monitoring of vibration signatures," *23rd International Conference on Industrial Electronics, Control and Instrumentation*, Vol. 3, pp. 1124-1129, Nov 1997.

[17] Hailu, B., Gachagan, A., Hayward, G., and A. McNab, "Embedded piezoelectric transducers for structural health monitoring," *Proceedings of IEEE Ultrasonics Symposium*, Vol.1, pp. 735 –738, 1999.

[18] Hailu, B., Hayward, G., Gachagan, A., McNab, A., and R. Farlow, "Comparison of different piezoelectric materials for the design of embedded transducers for structural health monitoring applications," *IEEE Ultrasonics Symposium,* Vol. 2, pp. 1019-1012, 2000.

[19] Condition Monitoring and Diagnostic Engineering Management (COMADEM) International, http://www.comadem.com/frameset.htm (08/01/2003)

[20] Society of Machinery Failure Prevention Technology (MFPT), http://www.mfpt.org/ (08/01/2003)

[21] National Aeronautics and Space Administration (NASA), "Aviation Safety Program (AvSP)," http://www.grc.nasa.gov/WWW/avsp/about.htm (08/01/2003)

[22] National Aeronautics and Space Administration (NASA), "Vehicle Health Management (VHM)," http://www.grc.nasa.gov/WWW/cdtb/projects/vehiclehealth/index.html (08/01/2003)

[23] Office of Naval Research, "Science & Technology – Aircraft Technology," http://www.onr.navy.mil/sci_tech/special/351_strike/prog_aircraft.htm (08/01/2003)

[24] Department of Defense, "The Joint Strike Fighter Prognostics and Health Management," www.dtic.mil/ndia/2001systems/hess.pdf (08/01/2003)

[25] QinetiQ, "Vehicle Health and Usage Monitoring System," http://www.qinetiq.com/etc/medialib/docs/news_room/press_packs/defence.Par.0004.File.dat/DVD-TSSprel-D5(HK)_latest.doc (08/01/2003)

[26] QinetiQ, "Integrated Engine Management," http://www.qinetiq.com/news_room/newsreleases/2003/2nd_quarter/integrated0.html (08/01/2003)

[27] UK Department of Defense, http://www.mod.uk/business/excel/projects/rcsc05.htm (08/01/2003)

[28] US Army Material Systems Analysis Activity (AMSAA), "AMSAA Capabilities To Support Simulation-Based Acquisition (SBA)," http://www.amsaa.army.mil/sba/Sba_doc2.html (08/01/2003)

[29] CALCE Electronic Products and Systems Center, University of Maryland, College Park, http://www.calce.umd.edu/ (08/01/2003)

[30] Pennsylvania State University Applied Research Laboratory, http://www.arl.psu.edu/ (08/01/2003)

[31] The Boeing Company, "ETOPS Maintenance," *Aero Magazine*, No. 7, July 1999.

[32] Pecht, M., Dube, M., Natishan, M., and I. Knowles, "An Evaluation of Built-In Test," *IEEE Transactions on Aerospace and Electronic Systems*, Vol. 37, No. 1, pp. 266-272, January 2001.

[33] The Boeing Company, "New "Smart" Network to Reduce Boeing JSF Life-Cycle Costs," *Boeing News Release*, Washington, D.C., September 13, 1999. http://www.boeing.com/news/releases/1999/news_release_990913o.htm (08/01/2003)

[34] General Motors (Mcleish, James. G.), "Email Communication," Warren, Michigan, 9th April 2002.

[35] Ramakrishnan, A. and M. Pecht, "Implementing a Life Consumption Monitoring Process for Electronic Product, *IEEE Transactions on Components and Packaging Technologies*, Vol. 26, No. 3, pp. 625-634, September, 2003.

[36] Pecht, M., Radojcic, R., and G. Rao, Guidebook for Managing Silicon Chip Reliability, CRC Press, Boca Raton, FL, 1999.

[37] Young, D. and A Christou, "Failure Mechanism Models for Electromigration," *IEEE Transactions on Reliability*, Vol. 43, No. 2, June 1994.

[38] Li., J., and A. Dasgupta, Failure Mechanism Models for Material Aging Due to Inter-Diffusion *IEEE Transactions on Reliability*, Vol. 43, No. 1, March 1994.

[39] Rudra, B., and D. Jennings, "Tutorial: Failure-Mechanism Models for Conductive-Filament Formation," *IEEE Transactions on Reliability*, Vol. 43, No. 3, September 1994.

[40] Dasgupta, A., "Failure Mechanism Models For Cyclic Fatigue," *IEEE Transactions on Reliability.*, Vol. 42, No. 4, pp. 548-555, December 1993.

[41] Pecht, M., Lall, P., and E. Hakim, "The Influence of Temperature on Integrated Circuit Failure Mechanisms," *Quality and Reliability Engineering Intl*, Vol. 8, pp. 167-175, 1992.

[42] Miner, M.A., "Cumulative Damage in Fatigue," *Journal of Applied Mechanics*, pp. A-159 to A-164, September 1945.

[43] SAE J1211, Recommended Environmental Practices for Electronic Equipment Design, Rev. November 78.

[44] Monthly Temperature Averages for the Washington, DC Area, *http://www.weather.com/weather/climatology/monthly/USDC0001* (08/01/2003)

[45] Engelmaier, W., "Generic Reliability Figures of Merit Design Tools for Surface Mount Solder Attachments," *IEEE Transactions of CHMT*, Vol. 16, No. 1., pp. 103-112, 1993.

[46] Dallas Instruments, SAVER™ User's Manual, Dallas, Texas, February 2000.

[47] Bendat, S.J. and A.G. Piersol, Random Data: Analysis and Measurement Procedures, Wiley-Interscience, New York, NY, 1971.

[48] Collins, J., Failure of Materials in Mechanical Design, John Wiley & Sons, New York, NY, 1993.

[49] Cluff, K.D., "Characterizing the Commercial Avionics Thermal Environment for Field Reliability Assessment," *Journal of the Institute of Environmental Sciences*, Vol. 40, No. 4, pp. 22-28, Jul.-Aug. 1997.

[50] Anzai, H., "Algorithm of the Rainflow Method," pp. 11-20, The Rainflow Method in Fatigue, Butterworth-Heinemann, Oxford, 1991.

[51] Fuchs, H.O., Nelson, D.V., Burke, M.A., and T.L. Toomay, "Shortcuts in Cumulative Damage Analysis," *SAE National Automobile Engineering Meeting*, Detroit, 1973.

[52] Ramakrishnan, A., "Health and Life Consumption Monitoring Using Sensor Technologies," Masters' Thesis, University of Maryland, 2001

[53] Mishra, S., Pecht, M., Smith, T., McNee, I., and R. Harris, "Life Consumption Monitoring Approach for Remaining Life Estimation", *European Microelectronics Packaging and Interconnection Symposium, IMAPS*, pp. 136-142, Cracow, Poland, June 2002.

[54] IPC, "IPC J-STD-029" Performance and Reliability Test Methods for Flip Chip, Chip Scale, BGA, and other Surface Mount Array Package Applications," February 2000.

[55] MEG-Array, "Solder Joint Reliability Testing Results Summary, IPC-SM-785," http://www.fciconnect.com/pdffiles/highspeed/MEG-Array_IPC-SM-785_Results.pdf (08/01/2003)

[56] Collins, J., Failure of Materials in Mechanical Design, John Wiley & Sons, New York, NY, 1993.

[57] Anzai, H., “Algorithm of the Rainflow Method,” pp. 11-20, The Rainflow Method in Fatigue, Butterworth-Heinemann, Oxford, 1991.

[58] Constable, J. H., “Electrical Resistance as an Indicator of Fatigue,” *IEEE Transactions on Components, Hybrid and Manufacturing Technology*, Vol. 15, No. 6, December 1992.

[59] Institute for Interconnecting and Packaging Electronic Circuits, “IPC SM-785” Guidelines for Accelerated Reliability Testing of Surface Mount Solder Attachments," Lincolnwood, IL, July 1992.

[60] D. S. Steinberg, Vibration Analysis for Electronic Equipment, John Willey & Sons, New York, NY, 1988.